For Reference

NOT TO BE TAKEN FROM THIS ROOM

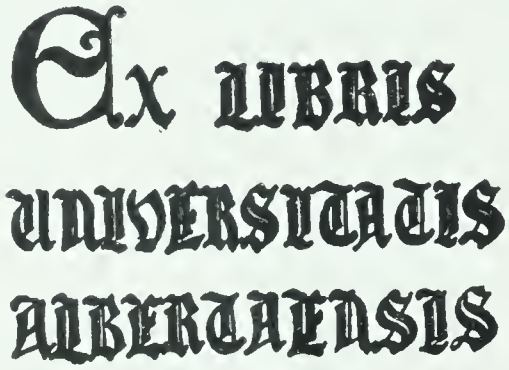

University of Alberta
Printing Department

Digitized by the Internet Archive
in 2019 with funding from
University of Alberta Libraries

https://archive.org/details/Hasegawa1962

1962 (F)
#31

THE UNIVERSITY OF ALBERTA

MAGNETO-TELLURIC STUDIES IN CENTRAL ALBERTA

by

Henry Hasegawa

A THESIS

SUBMITTED TO THE FACULTY OF GRADUATE STUDIES

IN PARTIAL FULFILMENT OF THE REQUIREMENTS FOR THE DEGREE

OF MASTER OF SCIENCE

DEPARTMENT OF PHYSICS

Edmonton, Alberta

September, 1962

MAGNETO-TELLURIC STUDIES IN CENTRAL ALBERTA

ABSTRACT

Magneto-telluric records were taken at five locations in central Alberta. The data were analyzed by the method outlined by Blackman and Tukey (1958). The data processing was done entirely by electronic means. An interpretation was carried out by employing Cagniard's theory in conjunction with information about the substructure obtained from other geophysical and geological methods.

For the sedimentary basin, resistivities ranging from 6 to 50 ohm meters were obtained. Moreover, the results indicate this basin to be horizontally isotropic. For the Precambrian, resistivities ranging from 600 to 10^6 ohm meters were obtained. The results indicate the Precambrian to be horizontally anisotropic. No electrical discontinuity was observed at depths ranging from 40 to 50 km. This suggests that there is no electrical discontinuity at the Mohorovicic discontinuity. From seismic evidence, the depth to this discontinuity was determined to be 43 km at Irricana. However, the results are suggestive of an electrical discontinuity at a depth of approximately 80 km.

ACKNOWLEDGMENTS

I wish to thank the following:

Dr. K. Vozoff for his supervision and assistance with various phases of this project.

Dr. G. D. Garland for his helpful suggestions.

R. M. Ellis for processing the field data.

M. D. Burke who designed and assembled the field apparatus.

P. Viney for assisting with the drawings.

Members of both the Computing Centre and the Geophysics Group (University of Alberta) who have assisted with various phases of this work.

The Alberta Society of Petroleum Geologists for permission to reproduce a regional geological cross section of the western Canada sedimentary basin.

The Petroleum Research Foundation of the American Chemical Society and the National Research Council for supporting this project.

TABLE OF CONTENTS

Page

Chapter I: Introduction. 1

Chapter II: The Magneto-Telluric Method (Cagniard 1953)

Outline of Method. 4

Frequency Range of Interest 5

Uniform Fields. 6

Classification and Origin of Micropulsations 8

Layering of Earth. 11

Displacement Current in a Conductor. . . 14

Direction of Propagation of Magneto-Telluric Wave in the Earth 14

Intrinsic Impedance of the Earth Which is Treated as a Semi-Infinite, Uniform Conductor. 16

Apparent Resistivity 17

Two-Layer Earth Model. 18

Five-Layer Model 21

Interpretation of Experimentally-Determined Apparent Resistivity Curves. 23

Price's Theory of Magneto-Telluric Methods. 26

General Theory. 26

Two-Layer Case with Extremely Resistive Substratum 29

Chapter III: Measurement of Magneto-Telluric Signals

General. 32

Field Instrumentation. 33

Absolute Coil Calibration. 40

Continued

Page

Playback Circuit. 43

Records of Magneto-Telluric Signals . . . 43

Chapter IV: Analysis of Magneto-Telluric Data

Introduction. 51

Outline of Mathematical Steps 52

Power Spectrum Graphs 57

Chapter V: Results and Interpretation .

Calculation of Experimental Resistivity. 64

Experimental Apparent Resistivity Curves. 64

Five-Layer Case. 65

Layer of Variable Conductivity. 68

Conclusion. 75

Appendix: Section I 77

Bibliography. 78

Table 1: Depth of Penetration Given in KM 7

Table II: Electrical Properties of Earth Materials. . . 7

Table III: Apparent Resistivity of the Sedimentary Formations Obtained from Electrical Logs. 69

Figure 1: Location of Magneto-Telluric Field Stations and Other Regions of Interest. 3

Figure 2a: Origin of Micropulsations. 10

Figure 2b: Location of Micropulsations on This Representation of Part of the Electro-Magnetic Spectrum. 10

Figure 3: Western Canada Sedimentary Basin 12

Continued

Page

Figure 4: Magneto-Telluric Regions of Interest. 15

Figure 5: Magneto-Telluric Standard Curves. 19

Figure 6: Instruments for Measuring Electric Field. . . 34

Figure 7: Block Diagram and Photographs of Instruments for Measuring Magnetic Field. 37

Figure 8: Equivalent Circuit for Magnetic Field Measurement. 38

Figure 9: Circuits for Calibrating Magnetic and Electric Components. 41

Figure 10a: Calibration Curves for Channels 5 & 6. . . . 42

Figure 10b: Calibration Curves for Electric and Magnetic Components. 42

Figure 11: Block Diagram and Photograph of Playback Circuit. 44

Figure 12: Bon Accord Magneto-Telluric Records 46

Figure 13: Bon Accord Magneto-Telluric Records. 47

Figure 14: Cooking Lake Magneto-Telluric Records 48

Figure 15: Cooking Lake Magneto-Telluric Records 49

Figure 16: Irricana Magneto-Telluric Records. 50

Figure 17a: Bon Accord Power Spectra Graphs. 59

Figure 17b: Bon Accord Power Spectra Graphs. 59

Figure 18a: Cooking Lake Power Spectra Graphs. 60

Figure 18b: Cooking Lake Power Spectra Graphs. 60

Figure 19a: Onoway Power Spectra Graphs. 61

Figure 19b: Onoway Power Spectra Graphs. 61

Figure 20a: Kavanagh Power Spectra Graphs. 62

Figure 20b: Kavanagh Power Spectra Graphs. 62

Figure 21a: Irricana Power Spectra Graphs. 63

Figure 21b: Irricana Power Spectra Graphs. 63

Continued

Page

Figure 22: Theoretical Apparent Resistivity Curves and Actual Earth Models - Leduc and Willingdon. 70

Figure 23: Experimental and Theoretical Apparent Resistivity Curves - Cooking Lake . . . 71

Figure 24: Experimental and Theoretical Apparent Resistivity Curves - Onoway. 72

Figure 25: Experimental and Theoretical Apparent Resistivity Curves - Bon Accord 73

Figure 26: Experimental Curves - Kavanagh 74

Figure 27: Experimental Curves - Irricana 74

CHAPTER I

INTRODUCTION

An investigation of the subsurface was carried out in central Alberta by using a geophysical exploration method termed "the magneto-telluric method" (Cagniard, 1953). The results obtained were compared with those from geological and other geophysical investigations.

A brief description of pertinent subsurface properties will now be given. Extensive knowledge of the structure and composition of the top layer, which is referred to as the western Canada sedimentary basin, has been obtained from seismic records and from well samples. Moreover, the resistivities of the sedimentary formations in central Alberta are obtainable from numerous electrical logs. Hence a comparison of the average resistivity and thickness of this layer as obtained by the magneto-telluric method, with those from in situ measurements is possible. Underlying the sedimentary basin, which is 2.7 km thick in the Edmonton area, is the Precambrian Shield. A combined geophysical and petrological study of the Precambrian in central Alberta by Garland and Burwash (1959) shows the lithology of the basement to vary over this area. Investigation of the subsurface at great depths has been carried out in Alberta at two different locations and by different geophysical methods. At Meanook, Niblett and Sayn-Wittgenstein (1960),

by employing the magneto-telluric method have detected a discontinuity in resistivity at a depth of 80 km. Seismic records at Irricana (Richards and Walker, 1959) indicate the depth to the Mohorovicic discontinuity to be 43 km.

Beneath the Precambrian lies the mantle, for which our knowledge of the composition and structure is limited mainly to information obtainable from seismic records.

Magneto-telluric recordings were taken at Irricana, Bon Accord, Onoway, Cooking Lake and Kavanagh in the summer and fall of 1961. In Figure 1 are shown the locations of the above-mentioned places together with the locations of wells in Alberta which have penetrated into the basement.

The results obtained by the magneto-telluric method were found to be consistent with those obtained by other methods.

▲ DEPTH TO ELECTRICAL DISCONTINUITY DETERMINED HERE

Fig. 1. Location of magneto-telluric field stations and other regions of interest.

CHAPTER II

THEORY

The Magneto-Telluric Method (Cagniard, 1953)

Outline of Method

Consider a region where the layers are homogeneous and horizontally stratified and where plane electromagnetic waves strike the surface. Then, providing adjacent layers have an appreciable electrical resistivity contrast and providing the signal has relatively strong harmonic components in the low frequency range (eg: 0.002 to 10 cps range), then the thickness and resistivity of each layer is obtainable by performing the following operations:

(1) measure simultaneously mutually perpendicular components (E_x and H_y say) of the electric and magnetic fields tangential to the earth's surface.

(2) process this data to determine those harmonic components which make a substantial contribution.

(3) compute the "apparent resistivity", ρ_a , for a number of values of the period, T, in the period range of interest by means of the following formula:

$$\rho_a = 2T \left| E_x/H_y \right|^2_{z=0} \quad \text{(em cgs units)} \qquad \ldots .\text{II - 1}$$

The ratio E_x/H_y is called the "intrinsic impedance" of the earth for plane waves (Schelkunoff, 1943).

The meaning of apparent resistivity and intrinsic impedance will be dealt with in a subsequent section.

(4) plot on transparent log-log paper apparent resistivity values against period.

(5) compare this curve with "master curves" computed from theoretical models and hence determine the "best-fit" curve.

(6) by means of a few simple operations (to be described later), determine the thickness and resistivity of each layer.

The advantage of Cagniard's method over electrical prospecting methods are two-fold. The depths of investigation are orders of magnitude greater than those dealt with in the latter method; neither power supplies nor base stations are required.

In theoretical work, many writers on this subject have employed electromagnetic units and in practical applications, "practical" units. Hence this procedure will be followed. A table for conversion from em cgs to practical units is given in the appendix (section I).

Frequency Range of Interest

This range is from 0.002 to 1 cps. In Figure 2(b) is shown the location of magneto-telluric signals in the electromagnetic spectrum. The reason for recording waves in this particular frequency range can be explained by

examining the concept of "skin depth" or "depth of penetration". It designates the depth to which an electromagnetic wave penetrates into a uniform conductor before its amplitude is reduced to 1/e of its surface value. The skin depth, p, is given by the familiar expression (in em cgs units)

$$p = \frac{1}{2\pi}\sqrt{\rho T} \quad . \qquad \ldots . \text{II - 2}$$

T = period in seconds
ρ = resistivity in em units
p = penetration in cms

In Table I is shown the skin depth for various periods and resistivities; in Table II is shown for typical materials, the skin depths at two periods.

In this investigation, the region of interest extends from the surface (sedimentary) layers to the top region of the mantle. In order to investigate the sedimentary basin, magneto-telluric signals with periods as small as 0.1 seconds are required; for mantle studies, periods of hundreds of seconds are required.

Uniform Fields

Investigation of telluric current records in France and in western Canada indicate these currents to be uniform over large areas.

In France, Blavier, upon examination of the telluric current records taken from parallel lines separated by as much as 270 kms, found them to be strikingly similar. Schlumberger and Kunetz (1948) found a correlation between

TABLE I

DEPTH OF PENETRATION GIVEN IN KM (After Cagniard)

ρ/T → ↓ ohm meters	1 sec	3 sec	10 sec	30 sec	1 min	2 min
0.2	0.225	0.390	0.712	1.23	1.74	2.47
1	0.503	0.872	1.59	2.76	3.90	5.51
5	1.13	1.95	3.56	6.16	8.72	12.3
10	1.59	2.76	5.03	8.72	12.3	17.4
50	3.56	6.16	11.3	19.5	27.6	39.0
250	7.95	13.8	25.2	43.6	61.6	87.2
1,000	15.9	27.6	50.3	87.2	123	174
5,000	35.6	61.6	113	195	276	390

TABLE II

ELECTRICAL PROPERTIES OF EARTH MATERIALS (After Garland)

Material	Typical resistivity, ohm meters	Depth of penetration* T = 1 sec km	T = 1 min km	T = 1 day km
Sea-water	.20	0.22	1.7	64.5
Unconsolidated soils	50.00	3.55	27.5	1040
Sedimentary rocks	100.00	5.03	38.9	1480
Igneous rock	1 x 10⁴	50.3	389	14800
Mantle, 1000 km depth	1.00	0.50	3.9	147

*The depth of penetration is the depth within the material at which an electric or magnetic field of the period shown would be reduced to 1/e of its surface value.

telluric records taken in locations as far separated as France and Madagascar. Garland and Webster (1960) infer from telluric records in western Canada that source distance effects are relatively unimportant. Simultaneous records of the E-W component of the electric signal taken in 1961 at Edmonton and Clive (N-S separation distance 75 miles) by the Universities of Alberta, British Columbia and California show a remarkable correlation.

However, at Meanook, investigation of magneto-telluric records by Niblett and Sayn-Wittgenstein (1961) indicate that source effects may be important for that location.

For this investigation, interpretation of the results will be made by assuming that the waves are uniform over lateral distances of at least 50 kilometers and that the material in each layer is isotropic.

Then the electric (E) and the magnetic (H) components are orthogonal and consequently obey the following:

$$E_x/H_y = E_y/H_x \qquad \ldots .II - 3$$

x = N-S component
y = E-W component

However, if the results indicate that the above relations do not apply, then source and anisotropic effects will be considered.

Classification and Origin of Micropulsations

Benioff (1960) has observed that magneto-telluric records usually occur in a variety of distinct types, each with its own features. In Figure 2b are shown pictorial representations

of the four main types (A, B, C, & D).

Type A Waves

These have periods up to several seconds and often persist up to 48 hours. The amplitudes of these waves are often modulated by longer period waves and are then described as "pearly".

Type B Waves

These have a period from 2 to 10 seconds. They are connected with auroral activity and are related to magnetic activity on the earth's dark side.

Type C Waves

These range in period from 8 to 40 seconds. Since they appear only on the sunlit side, they are called "day-time" activity. It is thought that this type modulates Type A to form pearls.

Type D Waves

The period range is from 40 to several hundred seconds. On occasion, long trains of these waves have been observed; at other times, they occur as a single pulse.

In Figure 2(a) are shown two different ways in which micropulsations are thought to originate.

Other means have been observed by which low frequency waves are generated. For example, waves with frequencies around 10 cps are the resonant frequencies of the electromagnetic cavity formed between the conducting earth and the ionosphere. Lightning probably starts this cavity ringing (Balser and Wagner, 1960).

ORIGIN OF MICROPULSATIONS may be far out in earth's magnetic field or near the earth in the ionosphere. At top, wave generated far away by protons from the sun moves toward earth as a hydromagnetic wave, traverses ionosphere (*color*), changes to long electromagnetic wave (*solid line*) and strikes earth. At bottom, solar protons come in close, generating long wave in the ionosphere.

Fig. 2(a)

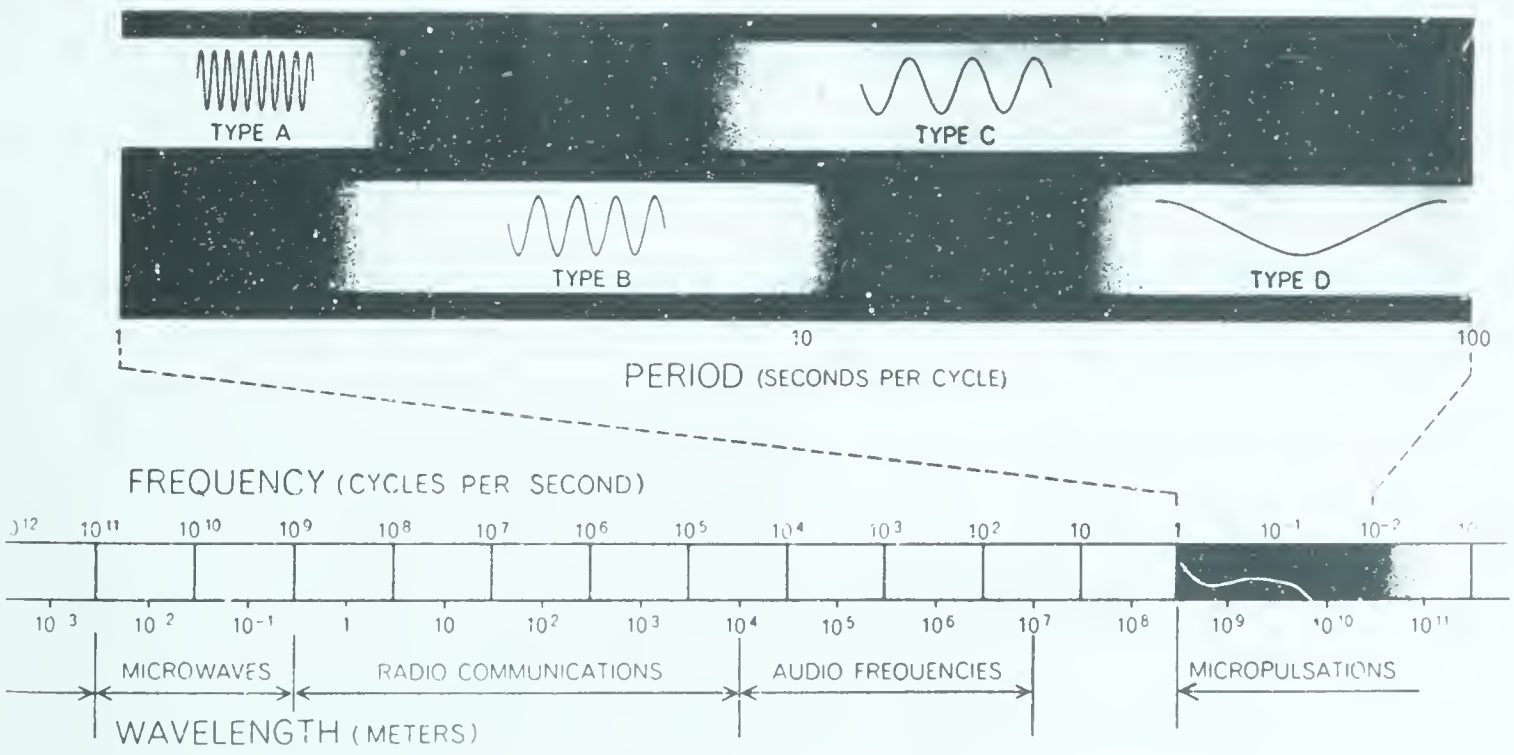

Location of micropulsations on this representation of part of the electromagnetic spectrum (after Heirtzler, 1962).

Fig. 2(b)

Hence the components of micropulsations have diverse origins and the determination of their origins is, in general, complicated by the presence of the ionosphere.

Layering of Earth

Cagniard's method is especially suited to regions of horizontal layering of fairly homogeneous, isotropic properties.

In Figure 3 is reproduced a geological cross section of the western Canada sedimentary basin. This cross section commences at Nordegg (see Figure 1) which is in the Alberta foothills and passes through Leduc (20 miles south of Edmonton). This line is approximately perpendicular to the Rocky Mountains. Taking into account the fact that the vertical scale exaggeration is approximately 42 times, the layering can be seen to be approximately horizontal and of fairly uniform thickness over large lateral distances.

Examinations of electric logs taken at numerous locations in central Alberta indicate that the layering in the sedimentary basin is, in general, electrically inhomogeneous. That is, the apparent or mean resistivity for a given layer was found to vary at different locations. However, over regions of horizontal extent of say 50 to 80 miles, this change is probably negligible. Hence, for apparent resistivity calculations, the layers were assumed to be homogeneous.

From geological investigations, the sedimentary basin is thought to be horizontally isotropic. Anistropic media are observed mainly in shales, which often have mineral

G

FOOTHILLS

RIMBEY-MORINVILLE
Reef Chain

H

INTERSECTION SECTION NLHCO

NORDEGG
EL 4471'

North Saskatchewan River

PEMBINA FIELD
(Projected)
3000 Wells

LEDUC FIELD
(860 Wells)

REDWATER FIELD
(916 Wells)

WILLINGDON FIELD
(Wet Gas)

North Saskatchewan River

Wolf Creek

Modeste Creek

Beaver Creek

5000
4000
3000
2000
1000
SEA LEVEL
-1000
-2000
-3000
-4000
-5000
-6000
-7000
-8000
-9000
-10000
-11000
-12000

EDMONTON
BELLY RIVER
LEA PARK
WAPIABI
CARDIUM
BLACKSTONE
COLORADO
LUSCAR
PASKAPOO
(Paleocene)
EDMONTON
BEARPAW
BELLY RIVER
BASAL SS
1st WHITE SPECKS
LEA PARK
COLORADO
WAPIABI
CARDIUM
BLACKSTONE
2nd WHITE SPECKS
BASE FISH SCALE
BLAIRMORE
MISSISSIPPIAN
UPPER DEVONIAN
LUSCAR
NORDEGG
FERNIE
BANFF
WABAMUN
EXSHAW
GRAMINIA
CALMAR
ELKTON SHUNDA
DYSON
PALLISER
NISKU
ALEXO
FAIRHOLME
IRETON
(Green shale)
DUVERNAY
ELK POINT
GHOST RIVER
UPPER CAMBRIAN 4-15
MIDDLE CAMBRIAN
PRECAMBRIAN
(>2000 m.y.)
CADOMIN
FERNIE
NORDEGG
RUNDLE
TWP 85
5TH MERIDIAN
TWP 30
TWP 55

Q=8Ωm
7
UPPER CRETACEOUS
6
4
LOWER CRETACEOUS
4-9
15
25
10
30
100
30
4-15

VARIEGATED & PALE BEDS
GRIZZLY BEAR
LEA PARK
COLORADO
DUVERNAY
IRETON
LEDUC
WATT MTN
WINNIPEGOSIS
"ELM POINT"
NISKU
DUVERNAY
COOKING LAKE
BEAVERHILL LAKE
SLAVE POINT
1st SALT
2nd SALT
3rd SALT
MIDDLE DEVONIAN
(ELK POINT)
ASHERN
BASAL SS Memb.

AVERAGE RESISTIVITY

Regional Geological Cross Section
of the
WESTERN CANADA SEDIMENTARY BASIN

Scale : 1" to 24 miles (Hor.)
1" to 3000 feet (Vert.)

FIG. 3 Reproduced through courtesy of Alberta Society of Petroleum Geologists.

H
2

crystals of fairly elongated shape (mica, kaolin, etc) embedded in them. An electric current travels with greater facility along the interstices which may exhibit a parallelism with the stratification and which are usually saturated with the mineralized water. An experiment to test the ground (to a depth of 100 feet) for anisotropy was performed at Kavanagh. The results indicate the ground to be horizontally isotropic down to this depth.

The Precambrian in central Alberta has been investigated by Garland and Burwash (1960) in a combined gravitational and petrological study. Their results indicate the basement lithology to vary over this area and to consist of three main types; namely, gneissic, granitic and basic phases. Hence it would be incorrect to assume, a priori, that the electrical resistivity of the basement be the same at the various recording sites. Moreover, since relatively little is known of the electrical properties in situ of the basement, it is not known whether the basement is isotropic or anisotropic. Since micropulsations penetrate readily into the basement, the magneto-telluric method should be ideal for investigating the electrical properties of this region.

Very little is known about the electrical properties of the top portion of the mantle. From an analysis of magneto-telluric records taken at Meanook, Niblett and Sayn-Wittgenstein (1961) suggest that there may be an electrical discontinuity at a depth of 80 km.

Thus the subsurface of central Alberta probably consists of a highly resistive Precambrian sandwiched between two relatively conductive layers.

Displacement Current in a Conductor

It is evident from an inspection of Maxwell's relation:

$$\nabla \times \vec{H} = 4\pi \vec{J} + \vec{\dot{D}} \quad , \qquad \ldots .\text{II} - 4a$$

that in a conductor of conductivity σ and dielectric constant ϵ , there is both a conduction current and a displacement current. The right hand side of II - 4a can be written (for sinusoidal waves) as:

$$4\pi\sigma \vec{E} + i\omega\epsilon \vec{E} = (4\pi\sigma + i\omega\epsilon)\vec{E} \, . \qquad \ldots .\text{II} - 4b$$

The displacement current term becomes less important as the wave frequency is decreased. Figure 4 shows the magneto-telluric region (in so far as this investigation is concerned) and the region where the displacement current becomes appreciable in comparison with the conduction currents. Examination of the figure shows that in the region of interest, the displacement current is negligible. Henceforth, the displacement current term, when dealing with the earth, will be omitted.

Direction of Propagation of Magneto-Telluric Wave in the Earth

Consider a plane wave of propagation constant k_1 striking the earth at an angle of incidence θ_1. Let k_2 and θ_2 be the corresponding value for the refracted ray. From Snell's law:

$$\sin \theta_2 = \frac{K_1}{K_2} \sin \theta_1 \, . \qquad \ldots .\text{II} - 5$$

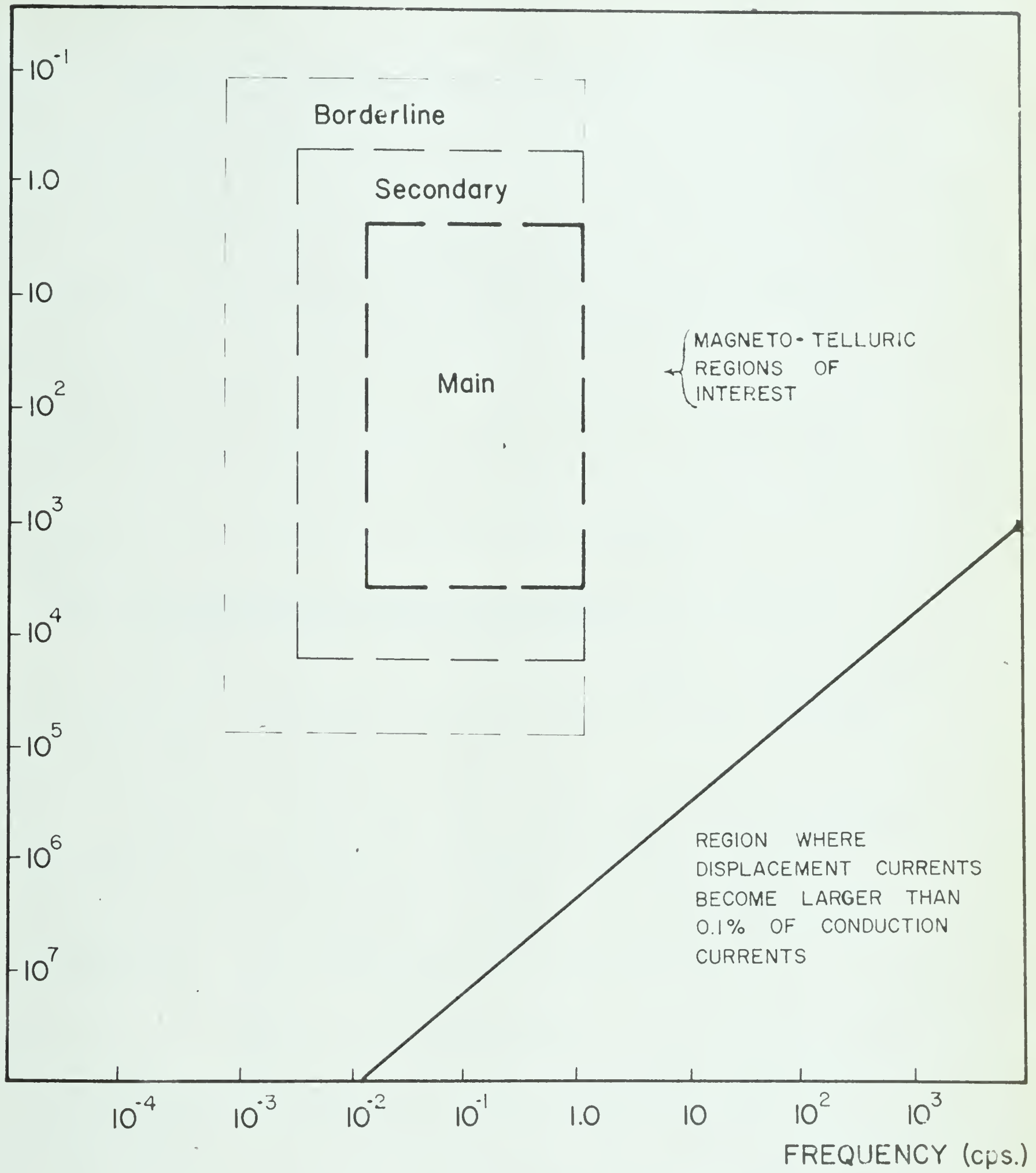

Fig. 4. Location of region where displacement current becomes larger than 0.1% of conduction currents (after Neves, 1957) and magneto-telluric regions of interest.

The wave equation is:

$$\nabla^2 \vec{H} = (4\pi i \omega \sigma - \omega^2 \epsilon)\vec{H} \quad \ldots\ldots \text{II - 6}$$

Hence $K_1^2 = -\omega^2\epsilon$ and $K_2^2 = 4\pi i \omega \sigma$ $\ldots\ldots$ II - 7

$$\therefore |\sin \theta_2| \leq \left|\sqrt{\frac{\omega^2 \epsilon}{4\pi\omega\sigma}}\right| |\sin \theta_1| \simeq 0$$

since the conduction current term (on the denominator) is much greater than the displacement current term (on the numerator) in the magneto-telluric region of interest. An inspection of Figure 4 shows this. Thus, no matter what the angle of incidence, the direction of propagation in the earth will be essentially vertically downward.

Intrinsic Impedance of the Earth which is Treated as a Semi-Infinite, Uniform Conductor

Cartesian co-ordinates with the X-Y plane on the earth's surface and Z pointing downwards will be used. X points towards the geographic north pole.

Consider a plane wave with the electric vector polarized in the N-S direction and the magnetic vector, in the E-W direction, impinging upon the earth. From Maxwell's curl relation II - 4, one obtains (for the conductor):

$$\frac{\partial \vec{H}_Y}{\partial z} = -4\pi\sigma \vec{E}_x \quad \ldots\ldots \text{II - 8}$$

From the wave equation II - 6, one obtains (for the conductor):

$$\vec{H}_Y = \vec{H}_{Yo}\, e^{-\sqrt{4\pi i\omega\sigma}\, z} \quad \ldots\ldots \text{II - 9}$$

The intrinsic impedance of a uniform earth for plane waves is defined as the ratio of E_x to H_y where:

$$\left.\frac{E_x}{H_y}\right|_{z=0} = (2\sigma T)^{-1/2}. \qquad \ldots .\text{II - 10}$$

Intrinsic impedance is analogous to the "characteristic impedance" of a one-dimensional transmission line. For free space, this impedance is 376.6 ohms.

The resistivity ρ can be expressed in terms of the intrinsic impedance and is given by II - 1.

After a brief discussion on apparent resistivity, it will be shown how equation II - 1 is used to interpret subsurface structure.

Apparent Resistivity

Consider two models: a Model (A) which is horizontally stratified into n electrically homogeneous layers of resistivities ρ_1, ρ_2, ... ρ_n, and also a Model (B) of uniform resistivity ρ_a. Consider a wave of period T which penetrates into the n^{th} layer of Model (A); let the intrinsic impedance for this Model be $E_x/H_y\,|_{z=0}$. Now let a wave with the same period T impinge upon Model (B).

Let ρ_a be of such a magnitude that the intrinsic impedance for Model (B) is the same as that for Model (A). Then ρ_a is called "apparent resistivity" for the n layers (for that particular value of T) and, physically, it is a measure of the mean or average of the resistivities of the n layers.

The Two-layer Earth Model

At certain locations, (eg: where the Precambrian Shield extends from the surface to the mantle) the earth approximates a two-layer model. In Figure 5(a) are shown graphs of apparent resistivity versus period (on log-log paper) for a number of resistivity values of the bottom layer, the upper layer being 1 kilometer thick and having a resistivity of 1 ohm meter.

The expression for the intrinsic impedance for plane waves, $E_x/H_y\big|_{z=0}$ is readily obtainable for the two-layer case from the five-layer case given by II - 18 by putting $p_5 = p_4 = p_3 = p_2$ and $h_4 = h_3 = h_2 = h_1$.

Two special case of interest will now be treated:

(a) the extremely resistive substratum case.

when $p_2 = \infty$, the expression for $E_x/H_y\big|_{z=0}$ becomes:

$$\left|\frac{E_x}{H_y}\right|_{z=0} = \sqrt{\frac{\rho_1}{2T}}\sqrt{\frac{\cosh(2h/p_1) + \cos(2h/p_1)}{\cosh(2h/p_1) - \cos(2h/p_1)}} \quad \ldots\ldots \text{II - 11}$$

where p_1 is the skin depth in the first medium and ρ_1 is its resistivity.

When $h \ll p_1$, II - 11 becomes:

$$\frac{E_x}{H_y}\bigg|_{z=0} = \frac{1}{2}\sqrt{\frac{\rho_1}{T}}\,\frac{\rho_1}{h_1} \quad . \qquad \ldots\ldots \text{II - 12}$$

The corresponding expression for ρ_a is:

$$\rho_a = \frac{\rho_1^2}{8\pi^2 h_1^2}\,T \quad . \qquad \ldots\ldots \text{II - 13}$$

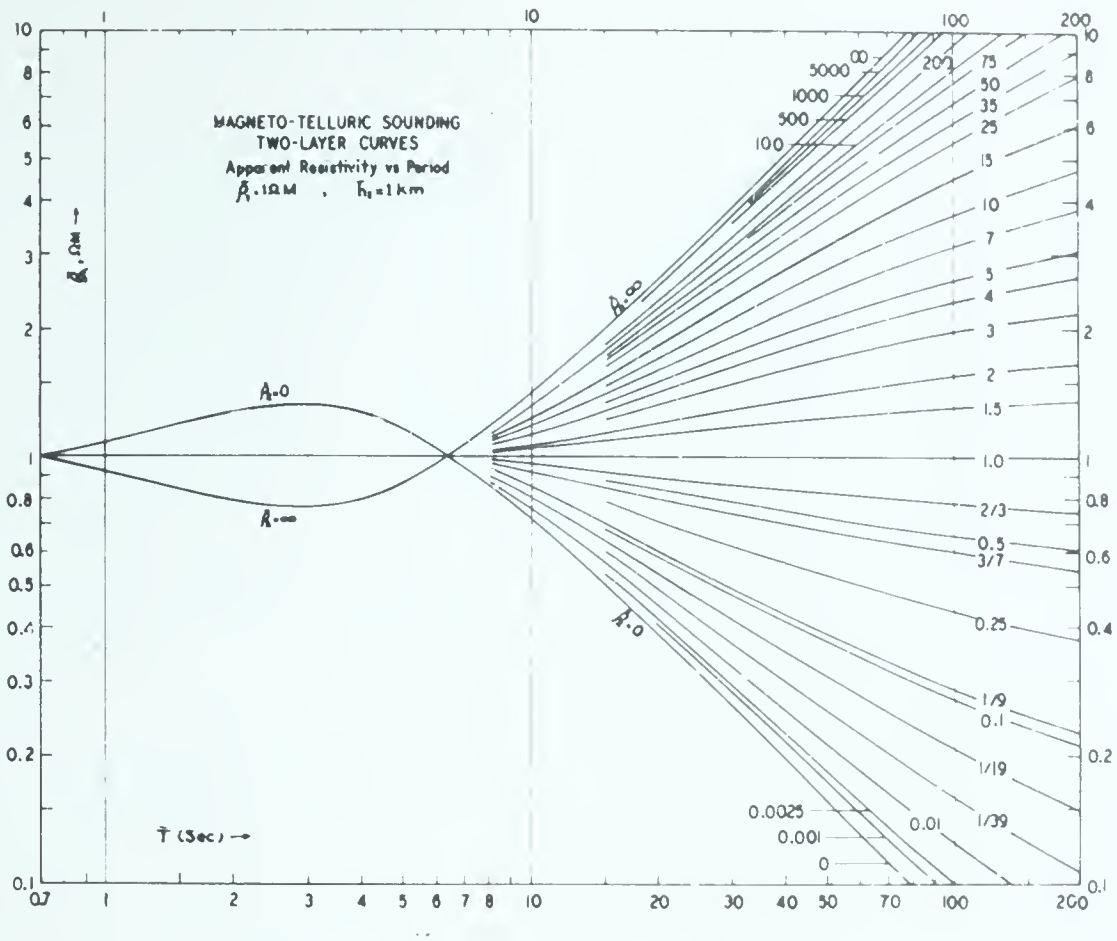

(a) Two-layer standard curves.

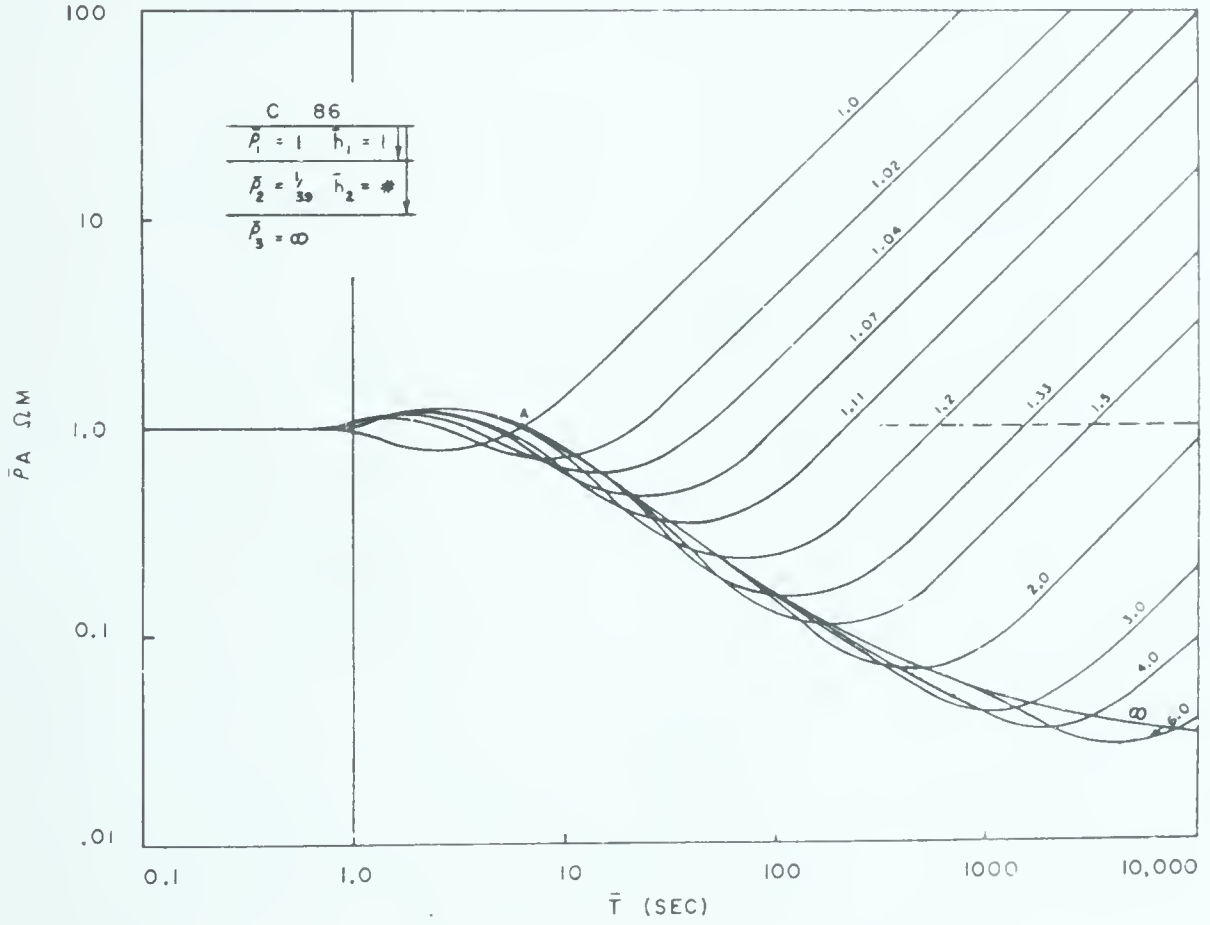

(b) Three-layer standard curves.

Fig. 5. Magneto-telluric standard curves (after Yungul, 1961).

An interesting feature of the graph of ρ_a versus T (when plotted on log-log paper) is observed for this case. As T increases, the graph of ρ_a versus T becomes linear and its slope makes an angle of 45^o with the abscissa. To see this, take the log of both sides of II - 13. One gets:

$$\log \rho_a = \log \left(\frac{\rho_1^2}{8\pi^2 h_1^2} \right) + \log T \quad \ldots .II - 14$$

Taking the derivative of both sides with respect to log T, one gets:

$$\frac{d}{d(\log T)} (\log \rho_a) = 1 \quad \ldots .II - 15$$

(b) <u>the extremely conductive substratum case.</u>

when $p_2 = 0$, the expression for E_x/H_y becomes:

$$\left| \frac{E_x}{H_y} \right|_{z=0} = \sqrt{\frac{\rho_1}{2T}} \sqrt{\frac{\cosh(2h_1/p_1) - \cos(2h_1/p_1)}{\cosh(2h_1/p_1) + \cos(2h_1/p_1)}} \quad \ldots .II - 16$$

when $h << p_1$,

$$\left| \frac{E_x}{H_y} \right|_{z=0} = \sqrt{\frac{\rho_1}{T}} \frac{h_1}{p_1} \quad \ldots .II - 17$$

The corresponding graph of ρ_a versus T for large values of T becomes linear and has a slope of -45^o.

For the cases where the experimental apparent resistivity curves (when plotted on log-log paper) have slopes with magnitudes greater than 45^o with respect to the abscissa, interpretation of sub-surface structure by Cagniard's method is not possible. Then such factors as source effects and anisotropy must be taken into account. However, it is only when these two effects can be dealt with individually that an interpretation becomes possible.

Five-Layer Model

An inspection of Figure 3 shows the sedimentary basin in the Leduc area to consist of rocks from five geological time divisions; they are the UPPER CRETACEOUS, the LOWER CRETACEOUS, the UPPER DEVONIAN, the MIDDLE DEVONIAN and the UPPER and MIDDLE CAMBRIAN periods. In order to determine the influence these five layers have on the shape of the apparent resistivity curve, expressions for the intrinsic impedance and the corresponding apparent resistivity were developed for a five-layer case. The following expressions (which are original calculations) were derived because previous calculations were for two or three layers only.

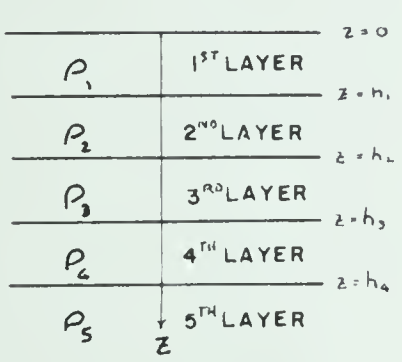

FIVE-LAYER EARTH SECTION

Let:

k = subscript denoting layer no.
h_k = depth to bottom of layer k
ρ_k = resistivity of layer k
T = period of wave
p_k = skin depth relative to layer k
$= \frac{1}{2\pi}\sqrt{\rho_k T}$.
ρ_a = apparent resistivity

Then:

$$\rho_a = \rho_1 \left[\frac{E_R^2 + E_I^2}{H_R^2 + H_I^2} \right] \qquad \text{II - 18}$$

where:

$$E_R = \sum_{J=1}^{8} \left[D_{2J-1} \cosh\theta_{2J-1} + (-1)^{J+1} D_{2J} \sinh\theta_{2J-1} \right] \cdot \cos\theta_{2J-1}$$

$$E_I = \sum_{J=1}^{8} \left[D_{2J-1} \sinh\theta_{2J-1} + (-1)^{J+1} D_{2J} \cosh\theta_{2J-1} \right] \cdot \sin\theta_{2J-1}$$

$$H_R = \sum_{J=1}^{8} \left[D_{2J-1} \sinh\theta_{2J-1} + (-1)^{J+1} D_{2J} \cosh\theta_{2J-1} \right] \cdot \cos\theta_{2J-1}$$

$$H_I = \sum_{J=1}^{8} \left[D_{2J-1} \cosh\theta_{2J-1} + (-1)^{J+1} D_{2J} \sinh\theta_{2J-1} \right] \sin\theta_{2J-1}$$

(cont'd)

and

$$D_1 = \left(\frac{1}{\rho_1}+\frac{1}{\rho_2}\right)\left(\frac{1}{\rho_2}+\frac{1}{\rho_3}\right)\left(\frac{1}{\rho_3}+\frac{1}{\rho_4}\right)\left(\frac{1}{\rho_4}\right)$$

$$D_2 = \left(\frac{1}{\rho_1}+\frac{1}{\rho_2}\right)\left(\frac{1}{\rho_2}+\frac{1}{\rho_3}\right)\left(\frac{1}{\rho_3}+\frac{1}{\rho_4}\right)\left(\frac{1}{\rho_5}\right)$$

$$D_3 = \left(\frac{1}{\rho_1}+\frac{1}{\rho_2}\right)\left(\frac{1}{\rho_2}+\frac{1}{\rho_3}\right)\left(\frac{1}{\rho_3}-\frac{1}{\rho_4}\right)\left(\frac{1}{\rho_4}\right)$$

$$D_4 = \left(\frac{1}{\rho_1}+\frac{1}{\rho_2}\right)\left(\frac{1}{\rho_2}+\frac{1}{\rho_3}\right)\left(\frac{1}{\rho_3}-\frac{1}{\rho_4}\right)\left(\frac{1}{\rho_5}\right)$$

$$D_5 = \left(\frac{1}{\rho_1}+\frac{1}{\rho_2}\right)\left(\frac{1}{\rho_2}-\frac{1}{\rho_3}\right)\left(\frac{1}{\rho_3}-\frac{1}{\rho_4}\right)\left(\frac{1}{\rho_4}\right)$$

$$D_6 = \left(\frac{1}{\rho_1}+\frac{1}{\rho_2}\right)\left(\frac{1}{\rho_2}-\frac{1}{\rho_3}\right)\left(\frac{1}{\rho_3}-\frac{1}{\rho_4}\right)\left(\frac{1}{\rho_5}\right)$$

$$D_7 = \left(\frac{1}{\rho_1}+\frac{1}{\rho_2}\right)\left(\frac{1}{\rho_2}-\frac{1}{\rho_3}\right)\left(\frac{1}{\rho_3}+\frac{1}{\rho_4}\right)\left(\frac{1}{\rho_4}\right)$$

$$D_8 = \left(\frac{1}{\rho_1}+\frac{1}{\rho_2}\right)\left(\frac{1}{\rho_2}-\frac{1}{\rho_3}\right)\left(\frac{1}{\rho_3}+\frac{1}{\rho_4}\right)\left(\frac{1}{\rho_5}\right)$$

$$D_9 = \left(\frac{1}{\rho_1}-\frac{1}{\rho_2}\right)\left(\frac{1}{\rho_2}-\frac{1}{\rho_3}\right)\left(\frac{1}{\rho_3}+\frac{1}{\rho_4}\right)\left(\frac{1}{\rho_4}\right)$$

$$D_{10} = \left(\frac{1}{\rho_1}-\frac{1}{\rho_2}\right)\left(\frac{1}{\rho_2}-\frac{1}{\rho_3}\right)\left(\frac{1}{\rho_3}+\frac{1}{\rho_4}\right)\left(\frac{1}{\rho_5}\right)$$

$$D_{11} = \left(\frac{1}{\rho_1}-\frac{1}{\rho_2}\right)\left(\frac{1}{\rho_2}-\frac{1}{\rho_3}\right)\left(\frac{1}{\rho_3}-\frac{1}{\rho_4}\right)\left(\frac{1}{\rho_4}\right)$$

$$D_{12} = \left(\frac{1}{\rho_1}-\frac{1}{\rho_2}\right)\left(\frac{1}{\rho_2}-\frac{1}{\rho_3}\right)\left(\frac{1}{\rho_3}-\frac{1}{\rho_4}\right)\left(\frac{1}{\rho_5}\right)$$

$$D_{13} = \left(\frac{1}{\rho_1}-\frac{1}{\rho_2}\right)\left(\frac{1}{\rho_2}+\frac{1}{\rho_3}\right)\left(\frac{1}{\rho_3}-\frac{1}{\rho_4}\right)\left(\frac{1}{\rho_4}\right)$$

$$D_{14} = \left(\frac{1}{\rho_1}-\frac{1}{\rho_2}\right)\left(\frac{1}{\rho_2}+\frac{1}{\rho_3}\right)\left(\frac{1}{\rho_3}-\frac{1}{\rho_4}\right)\left(\frac{1}{\rho_5}\right)$$

$$D_{15} = \left(\frac{1}{\rho_1}-\frac{1}{\rho_2}\right)\left(\frac{1}{\rho_2}+\frac{1}{\rho_3}\right)\left(\frac{1}{\rho_3}+\frac{1}{\rho_4}\right)\left(\frac{1}{\rho_4}\right)$$

$$D_{16} = \left(\frac{1}{\rho_1}-\frac{1}{\rho_2}\right)\left(\frac{1}{\rho_2}+\frac{1}{\rho_3}\right)\left(\frac{1}{\rho_3}+\frac{1}{\rho_4}\right)\left(\frac{1}{\rho_5}\right)$$

$$\theta_1 = h_1\left(\frac{1}{\rho_1}-\frac{1}{\rho_2}\right)+h_2\left(\frac{1}{\rho_2}-\frac{1}{\rho_3}\right)+h_3\left(\frac{1}{\rho_3}-\frac{1}{\rho_4}\right)+h_4\left(\frac{1}{\rho_4}\right)$$

$$\theta_3 = h_1\left(\frac{1}{\rho_1}-\frac{1}{\rho_2}\right)+h_2\left(\frac{1}{\rho_2}-\frac{1}{\rho_3}\right)+h_3\left(\frac{1}{\rho_3}+\frac{1}{\rho_4}\right)-h_4\left(\frac{1}{\rho_4}\right)$$

$$\theta_5 = h_1\left(\frac{1}{\rho_1}-\frac{1}{\rho_2}\right)+h_2\left(\frac{1}{\rho_2}+\frac{1}{\rho_3}\right)-h_3\left(\frac{1}{\rho_3}+\frac{1}{\rho_4}\right)+h_4\left(\frac{1}{\rho_4}\right)$$

$$\theta_7 = h_1\left(\frac{1}{\rho_1}-\frac{1}{\rho_2}\right)+h_2\left(\frac{1}{\rho_2}+\frac{1}{\rho_3}\right)-h_3\left(\frac{1}{\rho_3}-\frac{1}{\rho_4}\right)-h_4\left(\frac{1}{\rho_4}\right)$$

$$\theta_9 = h_1\left(\frac{1}{\rho_1}+\frac{1}{\rho_2}\right)-h_2\left(\frac{1}{\rho_2}+\frac{1}{\rho_3}\right)+h_3\left(\frac{1}{\rho_3}-\frac{1}{\rho_4}\right)+h_4\left(\frac{1}{\rho_4}\right)$$

$$\theta_{11} = h_1\left(\frac{1}{\rho_1}+\frac{1}{\rho_2}\right)-h_2\left(\frac{1}{\rho_2}+\frac{1}{\rho_3}\right)+h_3\left(\frac{1}{\rho_3}+\frac{1}{\rho_4}\right)-h_4\left(\frac{1}{\rho_4}\right)$$

$$\theta_{13} = h_1\left(\frac{1}{\rho_1}+\frac{1}{\rho_2}\right)-h_2\left(\frac{1}{\rho_2}-\frac{1}{\rho_3}\right)-h_3\left(\frac{1}{\rho_3}+\frac{1}{\rho_4}\right)+h_4\left(\frac{1}{\rho_4}\right)$$

$$\theta_{15} = h_1\left(\frac{1}{\rho_1}+\frac{1}{\rho_2}\right)-h_2\left(\frac{1}{\rho_2}-\frac{1}{\rho_3}\right)-h_3\left(\frac{1}{\rho_3}-\frac{1}{\rho_4}\right)-h_4\left(\frac{1}{\rho_4}\right)$$

Interpretation of Experimentally-Determined Apparent Resistivity Curves

Interpretation of experimental resistivity curves in terms of layering in the subsurface can be effected by employing "standard" curves such as are shown in Figure 5. Since this method requires the use of the law of electrodynamic similitude, a brief derivation of this law will be given.

Suppose the two models shown below are connected by the following relations:

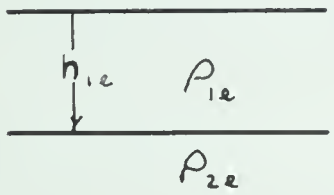

Earth Model

$$\rho_{1e} = K_\rho \rho_{1s} \qquad \text{- I}$$

$$\rho_{2e} = K_\rho \rho_{2s} \qquad \text{- II}$$

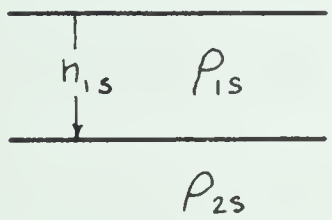

Standard Model

$$h_{1e} = K_L h_{1s} \qquad \text{- III}$$

$$T_e = K_T T_s \qquad \text{- IV}$$

. . . .II - 19

ρ = resistivity
h = thickness
T = period
K = dimensionless measure number

Consider two waves with equal amplitudes impinging upon both models. Then the law of similitude stipulates that the wave equation be satisfied for both models. That is:

$$\nabla_e^2 \vec{E} + i 4\pi \left(\frac{2\pi}{T_e}\right)\left(\frac{1}{\rho_e}\right) \vec{E} = 0 \qquad \text{(a)}$$

. . . .II -20

and also:

$$\nabla_s^2 \vec{E} + i4\pi\left(\frac{2\pi}{T_s}\right)\left(\frac{1}{\rho_s}\right)\vec{E} = 0 \quad . \qquad \text{(b)}$$

. . . .II - 20

By using equation (III), II - 19, one obtains:

$$\nabla_a^2 = \frac{1}{K_L^2}\nabla_s^2 \quad .$$

. . . .II - 21

Hence by using relations in II - 19, equation (a) of II - 20 can be transformed into the following form:

$$\frac{1}{K_L^2}\nabla_s^2 \vec{E} + i4\pi\left(\frac{2\pi}{K_T T_s}\right)\left(\frac{1}{K_\rho \rho_s}\right)\vec{E} = 0 \quad ,$$

or

$$\nabla_s^2 \vec{E} + i4\pi\left(\frac{2\pi}{T_s\rho_s}\right)\left(\frac{K_L^2}{K_T K_\rho}\right)\vec{E} = 0 \quad .$$

. . . .II - 22

This relation becomes identical to equation (b) of II - 20 when:

$$K_L^2 = K_T K_\rho \quad .$$

. . . .II - 23

This then is the condition which the dimensionless measure numbers must satisfy if the law of similitude is to hold.

Suppose now that one has an experimental apparent resistivity curve for a two-layered earth and one wishes to determine its parameters. Let the parameters be represented

by those of the earth model; let the standard model have p_1 = 1 unit and h_1 = 1 unit. Then the procedure for determining these parameters is as follows:

(1) place this experimental apparent resistivity curve (drawn on transparent paper) over the standard curves (Figure 5a) and translate it until a good fit is obtained.

(2) to obtain ρ_{1e}, read the value of the ordinate on the top graph which coincides with the curve $\rho_{1s} = 1$ on the bottom graph.

(3) to obtain ρ_{2e}, read the value of ρ_{2s} which best fits the experimental curve and multiply this value with ρ_{1e} .

(4) to determine h_{1e}, read the value of the abscissa (T_{1e}) on the top graph which coincides with $T_{1s} = 1$ on the bottom graph. Then from equations (III) of II - 19 and II - 23, one gets:

$$h_{1e} = K_L h_{1s} = \sqrt{K_T K_\rho}\, h_{1s}$$

Since $h_{1s} = 1$ and $\rho_{1s} = 1$,

$$K_T = T_{1e} \text{ and } K_\rho = \rho_{1e}.$$

$$\therefore h_{1e} = \sqrt{T_{1e}\rho_{1e}}. \qquad \ldots .\text{II - 24}$$

Hence an interpretation is obtained.

When the shape of the experimental apparent resistivity curve was suggestive of a two-layer case, the above method was used for an interpretation. However, many of the curves

were suggestive of three and four-layer cases; for such instances, theoretical apparent resistivity curves were obtained by using the formula for the five-layer case (II - 18). A computer program was written to determine theoretical apparent resistivity curves for layerings up to five in number and for any resistivity combinations.

Price's Theory of Magneto-telluric Methods When the Source Field is Considered

Although Price's theory (1962) is not used to obtain a quantitative interpretation of the experimental apparent resistivity curves obtained in this investigation, it is, nevertheless, suggested as a possible means of interpreting features of these curves that are difficult to explain by Cagniard's method. Consequently a brief description of Price's theory will be given.

Price took into account the nature of the source field in a general way. His method includes Cagniard's plane-wave treatment and Wait's (1954) dipolar source as special cases.

General Theory

Cartesian co-ordinates oriented with the X-Y plane on the earth's surface and Z vertically downwards will be chosen. For the present the earth will be treated as a semi-infinite conductor.

An expression for the intrinsic impedance $E_x/H_y|_{z=0}$

of the earth when the lateral dimensions of the source field are considered will be derived starting from Maxwell's equations. Neglecting displacement currents in the conductor and taking unity for the permeability of the earth, Maxwell's equation becomes:

$$\nabla \times \vec{H} = 4\pi \vec{I} = 4\pi \sigma(z) \vec{E} . \qquad \ldots .\text{II - 25}$$

$$\nabla \times \vec{E} = -i\omega \vec{H} . \qquad \ldots .\text{II - 26}$$

The wave equation obtained from the above equations in the usual manner is:

$$\nabla^2 \vec{E} = 4\pi i \omega \sigma(z) \vec{E} . \qquad \ldots .\text{II - 27}$$

In a previous paper (Lahiri and Price 1939), it was shown that currents induced in a conductor (where layers of equal conductivity are parallel to the surface) by an external field flow parallel to the surface. Although there is disagreement on this point, if one does accept it as being correct, then one obtains solutions to the wave equation of the form:

$$\vec{E} = e^{i\omega t} \vec{Z}(z) \vec{F}(x,y) , \qquad \ldots .\text{II - 28}$$

where:

$$\vec{F}(x,y) = \left(\frac{\partial P}{\partial y} , -\frac{\partial P}{\partial x} , 0 \right) . \qquad \ldots .\text{II - 29}$$

Substituting II - 28 and II - 29 into the wave equation II - 27, and employing the method of Separation of Variables, one gets:

$$\frac{\partial^2 P}{\partial x^2} + \frac{\partial^2 P}{\partial y^2} + \nu^2 P = 0, \qquad \ldots .\text{II - 30}$$

and

$$\frac{\partial^2 \vec{E}}{\partial z^2} = \left[\nu^2 + 4\pi i \omega \sigma(z) \right] \vec{E} \qquad \ldots .\text{II - 31}$$

Let:

$$\theta^2 = \nu^2 + 4\pi i \omega \sigma(z) . \qquad \ldots .\text{II - 32}$$

ν is a constant and the reciprocal of ν is shown by Price to be a measure of the horizontal extent of the source field. The range of the values for ν may be obtained by considering $2\pi/\nu$ as a measure of the linear dimension of the source field. The least value for ν is obtained when the source dimension is equal to the circumference of the earth. This case corresponds to the longest wavelength of the field. To obtain the greatest value for ν of practical importance, Price considers the case where the linear dimensions of the source are four times the height (100 kms) of the ionospheric jet currents. The range of ν thus obtained is 1.57×10^{-9}

to 1.57×10^{-7} cm^{-1}. Cagniard's case corresponds to taking ν equal to zero. Physically, this means that the lateral dimension of the source field is infinite; hence one is dealing with plane waves at the earth's surface.

The magnetic field obtained by using II - 28, II - 29, and II - 26 is:

$$\vec{H} = \frac{i e^{i\omega t}}{\omega} \left(\frac{dZ}{dz} \frac{\partial P}{\partial x}, \frac{dZ}{dz} \frac{\partial P}{\partial y}, \nu' Z P \right)$$

. . . .II - 33

The complex ratio $E_x/H_y\big|_{z=0}$ is obtained by using II - 28, II - 29 and II - 33, and is:

$$\frac{E_x}{H_y}\bigg|_{z=0} = -i\omega Z(0) \Big/ \frac{\partial Z}{\partial z}\bigg|_{z=0} .$$

. . . .II - 34

Two-layer Case with Extremely Resistive Substratum

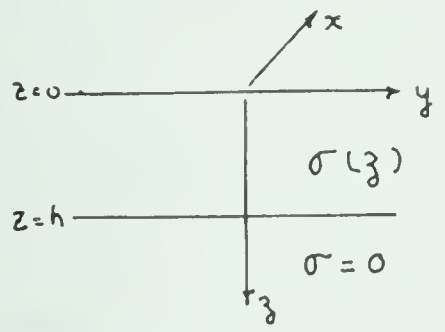

By employing relation II - 34 and the boundary conditions that the tangential components of E and H are continuous at z = 0 and h, one obtains for the intrinsic impedance the following:

$$\frac{E_x}{H_y}\bigg|_{z=0} = i\omega \frac{\theta + \nu + (\theta - \nu) e^{-2\theta h}}{\theta \left[\theta + \nu - (\theta - \nu) e^{-2\theta h} \right]} , \quad . . . .II - 35$$

where: $$\theta^2 = \nu^2 + 4\pi i\omega\sigma .$$

By putting $\nu = 0$ in II - 35, a result equivalent to Cagniard's II - 11 is obtained. In this case, one is dealing with plane waves.

When $h \to \infty$, II - 35 becomes:

$$\left.\frac{E_x}{H_y}\right|_{z=0} = \frac{i\omega}{\theta} = \frac{i\omega}{\sqrt{\nu^2 + 4\pi i\omega\sigma}} \quad \ldots .\text{II - 36}$$

when ν is small, II - 36 becomes:

$$\left.\frac{E_x}{H_y}\right|_{z=0} \approx \sqrt{\frac{i\omega}{4\pi\sigma}}\left(1 - \frac{\nu^2}{8\pi i\omega\sigma}\right) \quad \ldots .\text{II - 37}$$

Wait's expression for this case is:

$$\left.\frac{E_x}{H_y}\right|_{z=0} = \sqrt{\frac{i\omega}{4\pi\sigma}} + \frac{\sqrt{\frac{i\omega}{4\pi\sigma}}}{2\gamma^2 H_y}\left(\frac{\partial^2 H_y}{\partial y^2} - \frac{\partial^2 H_y}{\partial x^2} + 2\frac{\partial^2 H_x}{\partial x \partial y}\right) + \frac{O}{H_y}(\gamma^{-4}) \quad \ldots .\text{II - 38}$$

where $\gamma^2 = 4\pi i\omega\sigma$ is the square of the intrinsic propagation constant of the earth. Wait obtains the above expression by considering the field at the earth's surface to be composed of a superposition of elementary waves. His expression II - 38 reduces to that of Cagniard's II - 10 when the second order space derivative of the components of the magnetic field are small enough so that the second term on the right of II - 38 can be neglected in comparison

with the first. Wait's expression can be seen to correspond to II - 37 by using II - 33, II - 30 and II - 31. The ratio $E_x/\omega H_y$ varies as ν is increased from 0 to 10^{-6}. The larger ν is, the smaller $E_x/\omega H_y$ is and also the apparent resistivity .

An inspection of II - 32 shows that the relative importance of ν is greater the smaller the values of ω and σ. On the prairies, where the sedimentary strata have fairly high conductivity values, departure of the ρ_a vs T curves from those obtained by employing Cagniard's theory should be negligible for small periods. However at large periods, the departure may be significant. In places where the surface layer has a very small conductivity, such as the area to the east of the prairies, departure of the ρ_a vs T curves from Cagniard's should occur at shorter periods.

CHAPTER III

MEASUREMENT OF MAGNETO-TELLURIC SIGNALS

General

Measurements were made on the earth's surface of horizontal components of the total electric and magnetic fields. The geographic north-south and east-west components of these fields were measured. A component of the electrical potential gradient was determined by first measuring the voltage between two electrodes (driven into the ground) and then by dividing this voltage by the electrode separation distance (1,000 feet in this case). The corresponding magnetic component was determined by measuring the voltage induced in a coil by the varying magnetic field.

Two special properties of magneto-telluric signals are their very low frequencies and minute amplitudes. Because of the latter characteristic, these signals are also referred to as micropulsations. Electric fields are of the order of a hundred microvolts/kilometer; magnetic fields, of the order of a tenth of a gamma, where 1 gamma (γ) = 10^{-5} gauss (Γ). The intensity of the earth's field is in the range 0.25 to 0.75 gauss; thus the magnetic signals of interest are approximately 10^{-6} times that of the earth's main field.

Amplifiers used to record these micropulsations should have the following properties:

(1) Large Gain

Since the signals are recorded on magnetic tape

which has a minimum input level of 1 volt RMS, a gain in the order of thousands is required for the electric signal and hundreds of thousands for the magnetic signal.

(2) Low noise-level over the frequency range of interest

Components of micropulsations with frequencies greater than 0.2 cps have, in general, extremely small amplitudes. Hence, if an interpretation over the frequency range 0.002 to 1 cps is to be possible, the noise level must be very low in the 0.2 to 1 cps range.

(3) Stability at these long periods

The reason for recording the signals on magnetic tape is that the data could be analyzed entirely by electronic means, thereby eliminating what has hitherto been the most time-consuming part of the whole operation.

Field Instrumentation

(1) Detection of electric signal

A block diagram of the equipment is shown in Figure 6.

The electrodes were of copper tubing 2 feet in length and $1\frac{1}{2}$ inches in diameter. The electrode spacing was 1,000 feet. This type of electrode was chosen because:

(a) a good electrical contact with the ground could be obtained by simply driving the tubes into the ground.

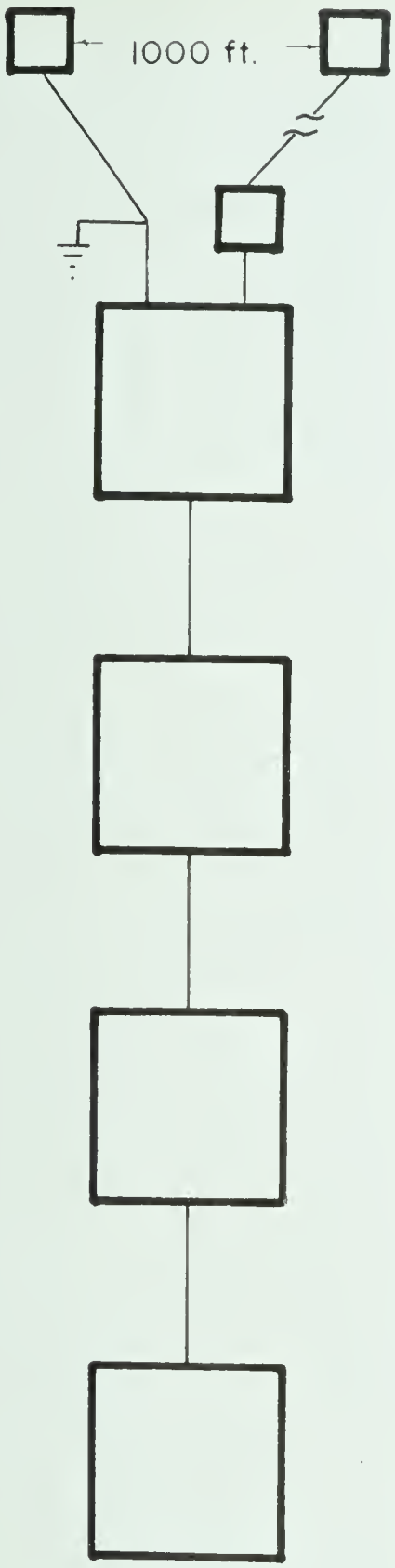

Fig. 6. Instruments for measuring Electric Field.

(b) although the electromotive force between copper and a solution of its salt is relatively large (-0.60 volts), changes in contact potential are negligible because of the short time interval (40 to 60 minutes) during which recordings were made.

A 220μf capacitor was inserted to block off any DC potential appearing across the electrodes. On the prairies, this potential is generally of the order of a few millivolts for an electrode spacing of 1,000 feet. The low-pass filter was inserted to eliminate the high-frequency components.

The amplifier, which received power from a 115v, 60 cps generator, has a maximum gain of 10,000. However, above a gain of 1,000, these amplifiers became unstable. Hence the gain was set at 1,000 for nearly all the records taken in the summer and fall of 1961.

Next a twin-T circuit with a zero transfer admittance at 60 cps was inserted to reject the 60 cps chopper frequency introduced by the amplifier. The characteristic impedance of the filter was 10,000 ohms.

Two devices were used to monitor the signals: they were a paper recorder (two-channel BRUSH RECORDER MARK II) and an oscilloscope (TECTRONIX TYPE 502 DUAL-BEAM). When the signal was observed

to have long period components of sufficient amplitudes, it was recorded on magnetic tape (PRECISION INSTRUMENT, PS-200 RECORDER). This frequency-modulated, 7-track record/reproducer has an error of ± ½db. The total harmonic distortion over the frequency range of interest is 1.5%. The input signal range is 1.0 volt RMS; the input impedance, 10,000 ohms.

(2) Detection of magnetic signal

A block diagram, together with photographs of some of the instruments is shown in Figure 7. The equivalent circuit is shown in the following figure.

Each coil was made of 30,000 turns of #26 wire wound around a highly permeable core(conetic - A.A.). To lessen wind noise, each coil was put in a shallow trench and covered with soil. A 30μf capacitor was inserted in parallel with the coil; the resulting coil resonant frequency was 1 cps. The voltage induced in each coil was generally less than a microvolt.

Next a galvanometer with a taut-band suspension and a current sensitivity of 3×10^{-8} amps/mm at 1 meter was inserted. A collimated beam of light was directed onto the galvanometer mirror from where it reflected onto a narrow gap between two silicon photoresistor cells. The latter have the special property of having an electrical resistivity

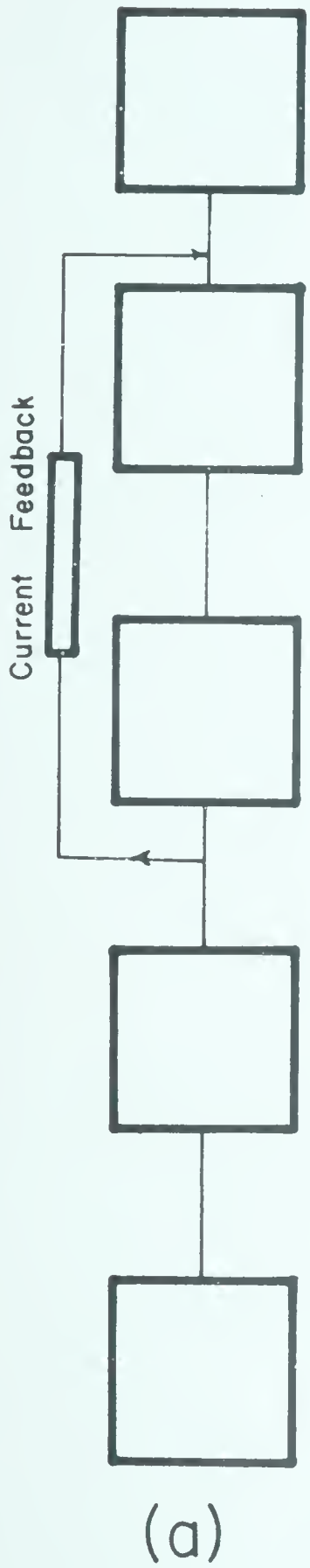

COIL
30,000 TURNS #26 Cu
CORE - CONETIC — A. A.

GALVANOMETER PLUS
PHOTORESISTOR CIRCUIT

DC AMPLIFIER
GAIN - 400

LOW - PASS FILTER
6 db REJECTION AT 2 cps.

FREQUENCY MODULATED
MAGNETIC TAPE RECORDER

(a) (b)

Fig. 7. Block diagram (a) and photographs (b) of instruments for measuring MAGNETIC field.

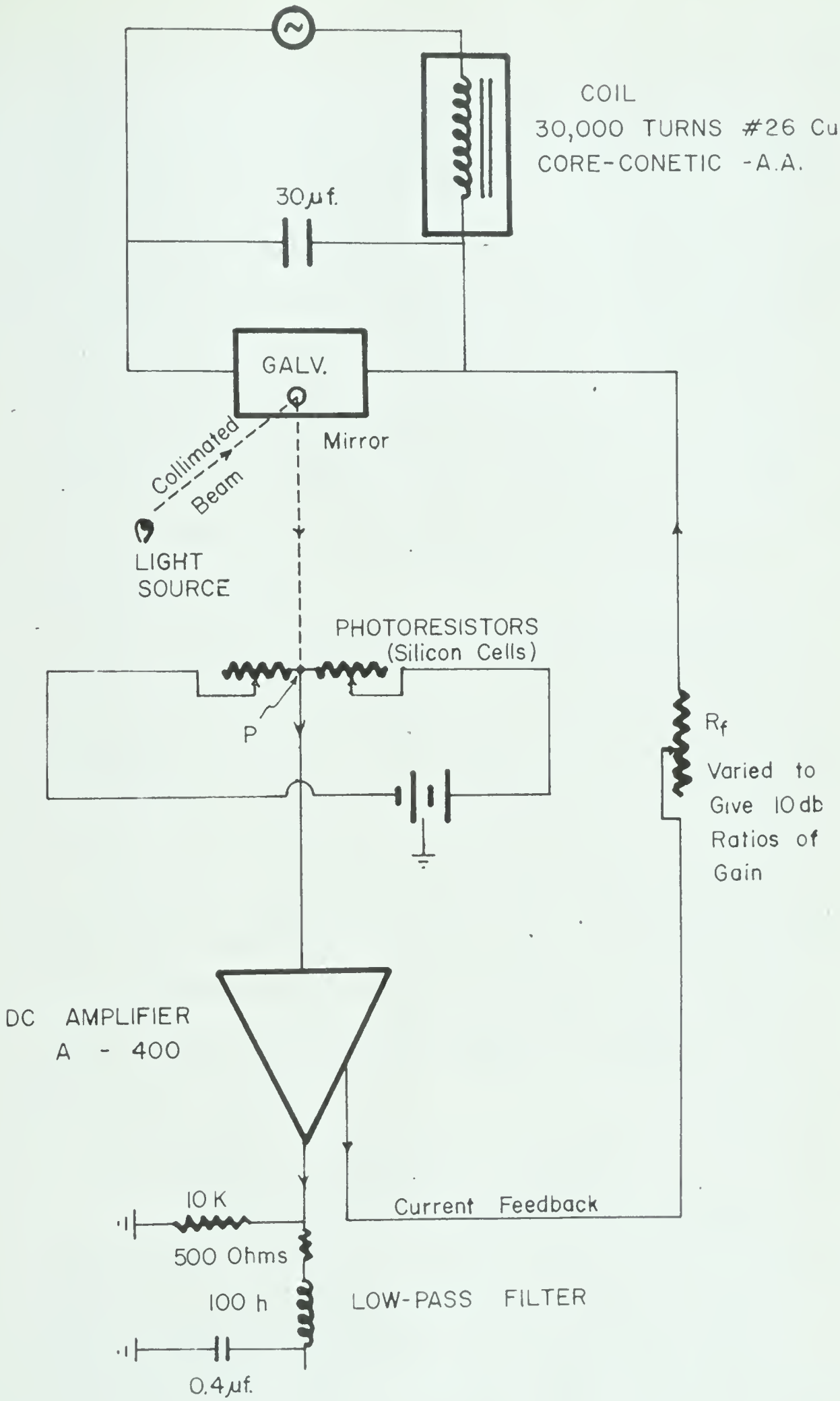

Fig. 8. Equivalent Circuit for Magnetic Field Measurement.

which depends very markedly upon the amount of light falling upon them. The greater the amount of light, the lower is their resistance. Hence, as can be seen from Figure 8, the potential at point P depends upon the current flowing through the galvanometer. This combination of photoresistor circuit and galvanometer constitutes the second stage of the amplification process, the first stage being that resulting from the highly permeable core.

The signal undergoes another amplification, this time by a DC amplifier. Part of this re-amplified signal is fed back to the galvanometer to null the current flowing through the latter.

By means of this three-stage amplification process, micropulsations of the order of a tenth of a gamma are amplified sufficiently so that they can be recorded on magnetic tape.

(3) Calibration Circuit

(a) Electric calibration circuit

In Figure 9 is shown the electric calibration circuit. A KROHN-HITE oscillator (Model 440A) was set at 1 volt RMS and the frequency was set at certain values in the range 0.01 to 10 cps. Two recordings on magnetic tape were made of this signal. One was the signal

appearing at the output of the oscillator and the other, the signal after passing through the amplifier circuit. Because a signal of 1 volt RMS is much too large for the amplifier, an attenuator was inserted. Calibration curves (volts out/millivolts in versus frequency) for the electric circuit are shown in Figure 10.

(b) Magnetic calibration circuit

This circuit is shown alongside the electric calibration circuit in Figure 9. A KROHN-HITE oscillator and a 600 ohm resistor were placed in series with the two-turn calibration loop. A calibration signal from this oscillator was sent through the two-turn loop at a number of frequencies in the range 0.01 to 10 cps. The signal at the output of the oscillator was put on magnetic tape; the calibration signal was also detected by the main coil, amplified and then recorded on magnetic tape. This calibration yields volts out/milliamp in the two-turn loop. The calibration curve for the magnetic circuits is shown in Figure 10b.

Absolute Coil Calibration

The above calibration circuits give volts out/milliamp in. In order to obtain volts out/gamma in, (in practical units, the magnetic field is measured in gammas) the box containing the main coil plus the two-turn loop was placed in a solenoid 10 feet in length, 1 foot in diameter and consisting of 300 turns. A signal from a low frequency oscillator

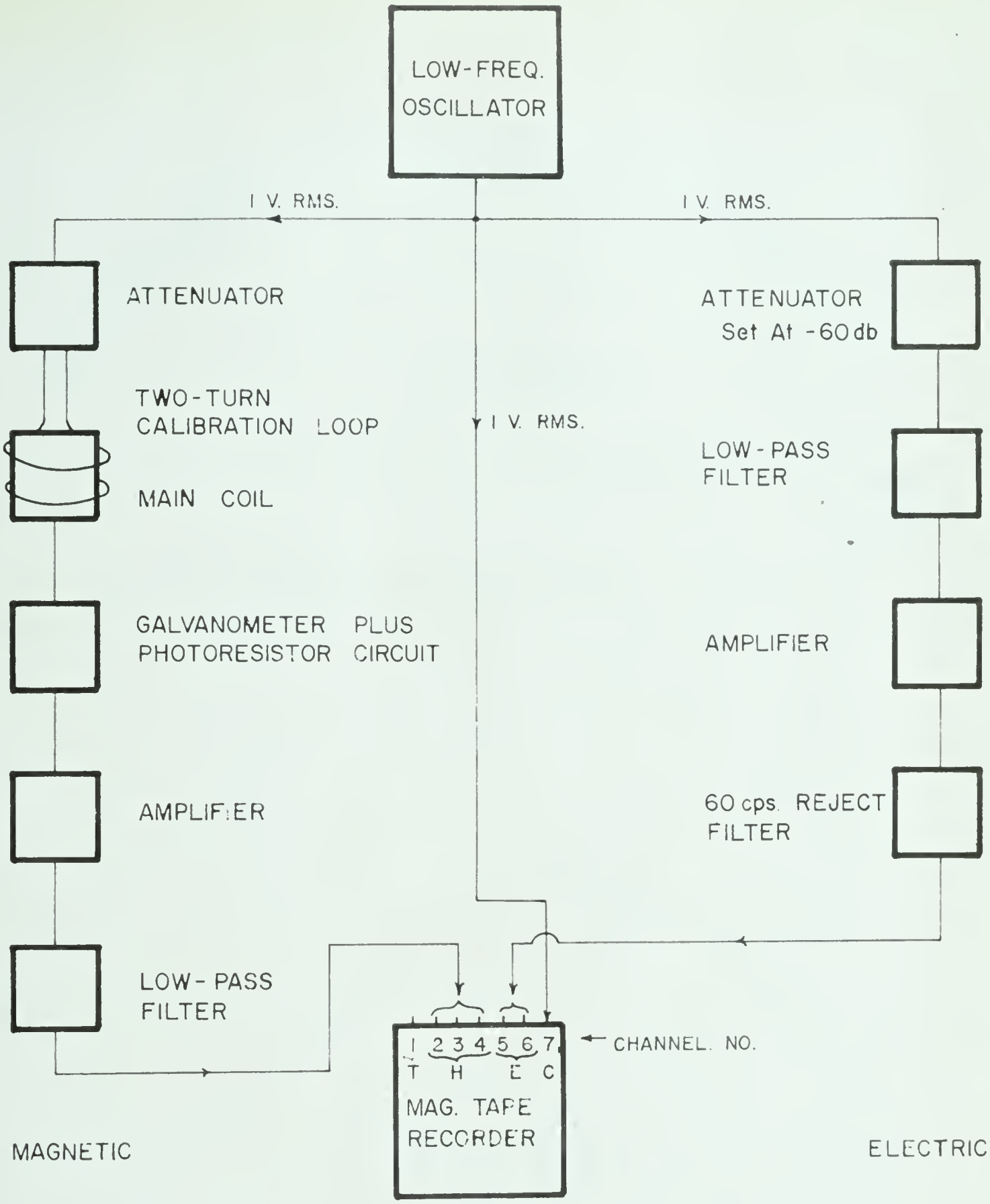

LEGEND

T - TIME

H - MAGNETIC COMPONENT

E - ELECTRIC COMPONENT

C - CALIBRATION

Fig. 9. Circuits for Calibrating Magnetic and Electric Components.

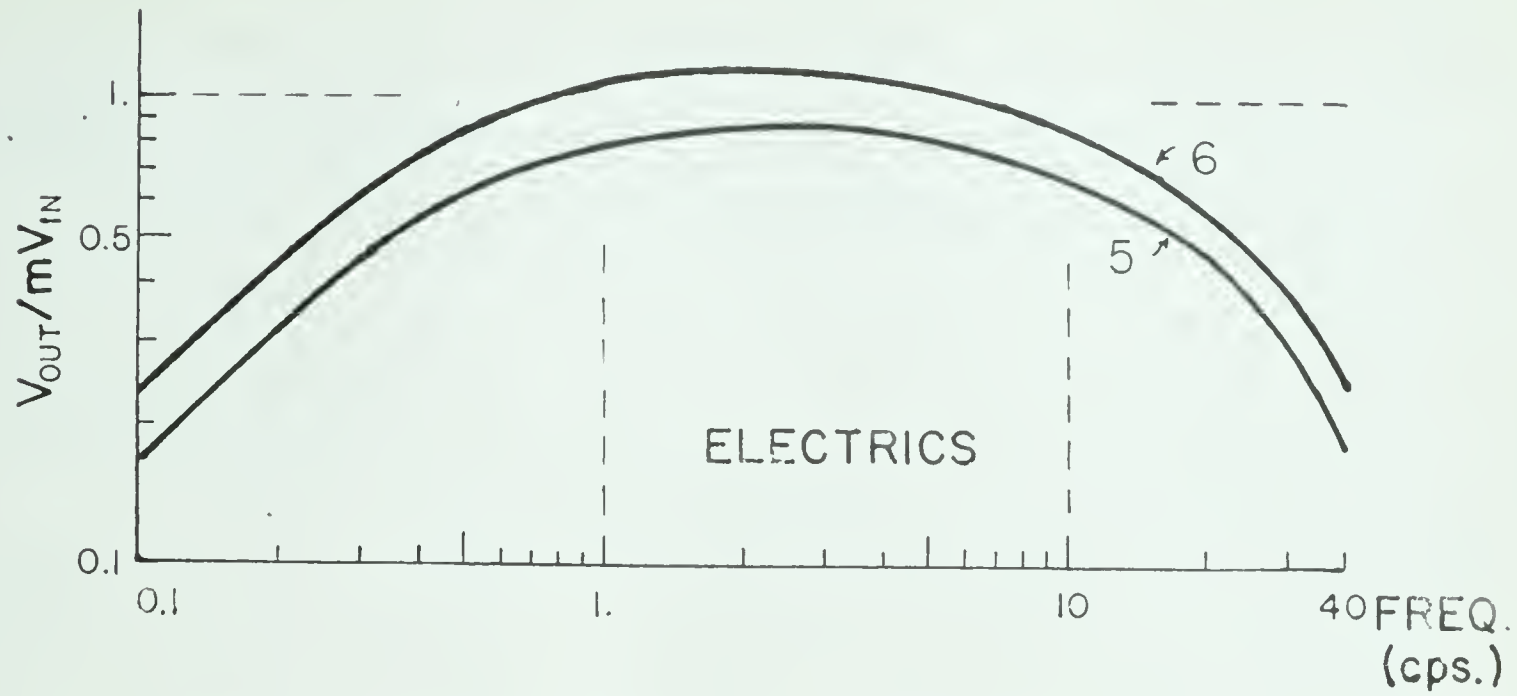

(a) Calibration Curves for Channels 5 and 6.

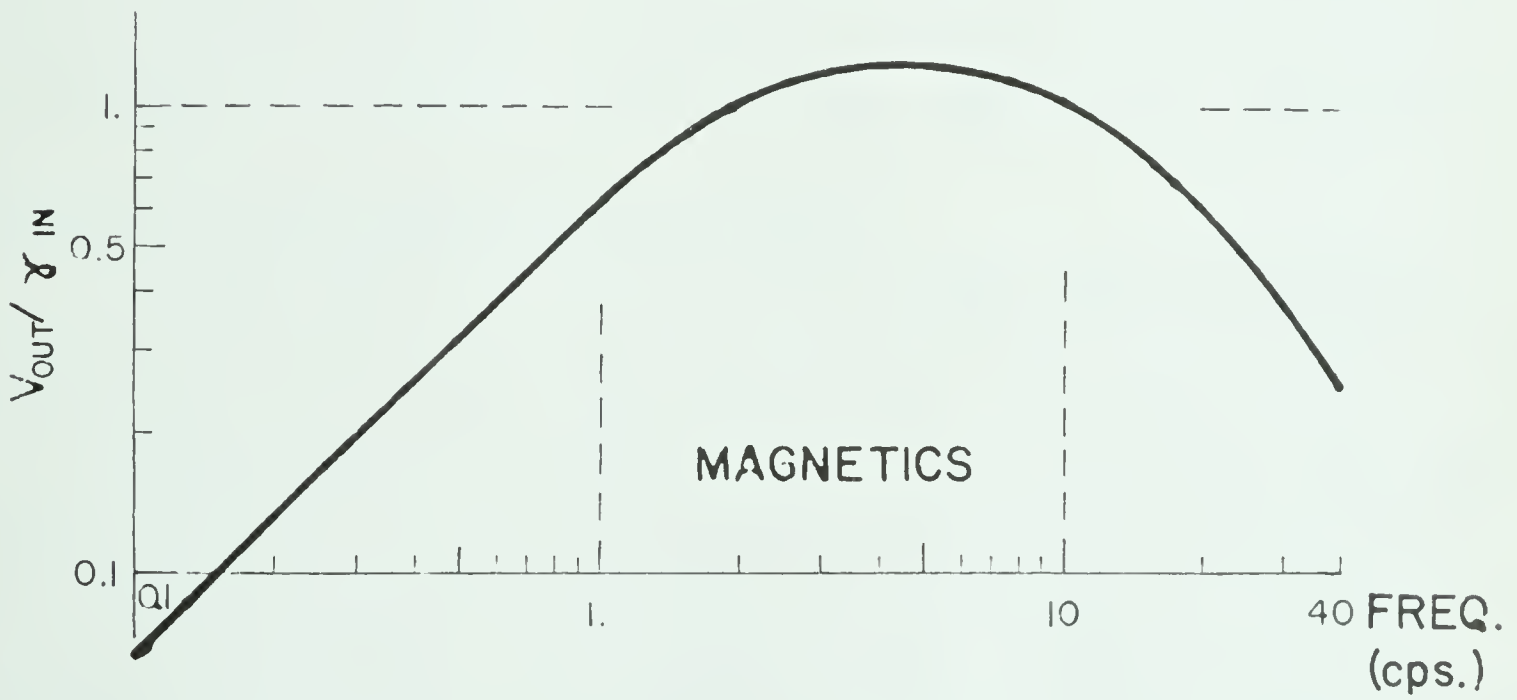

(b) Calibration Curve for Channels 2 and 3.

Fig. 10. Calibration Curves for Electric and Magnetic Components.

was passed through the two-turn calibration loop and the voltage induced in the solenoid circuit was measured. The magnetic flux passing through the solenoid could then be computed and was found to be 4.5 gammas/milliamp in the two-turn loop.

Playback Circuit

In Figure 11 are shown a diagram of the playback circuit together with a picture of the corresponding apparatus. The data (in analog form) on magnetic tape were digitized and recorded on paper tape. A Brush recorder was inserted in parallel with the circuit to monitor the signal being punched on paper tape. The SOROBAN TAPE PERFORATOR (Model GP2) records hole patterns at a maximum rate of 300 characters per second. The digitized data were now in a form whereby they could be read into the electronic computor (IBM 1620 at the University of Alberta) via the paper tape reader (IBM 1621).

Records of Magneto-Telluric Signals

In Figures12 to 16 are shown records taken in Central Alberta at Bon Accord, Cooking Lake and Irricana.

Components of magneto-telluric signals usually have very small amplitudes above a frequency of approximately 0.2 cps. Most of the records taken in the summer and fall of 1961 showed a lack of high frequency components in the range 0.2 to 1 cps. Exceptions were those taken at Bon Accord (Figures 12 and 13) and Cooking Lake (Figure 14 and 15). The magnetic components in Figure 12 show clearly the presence of a high

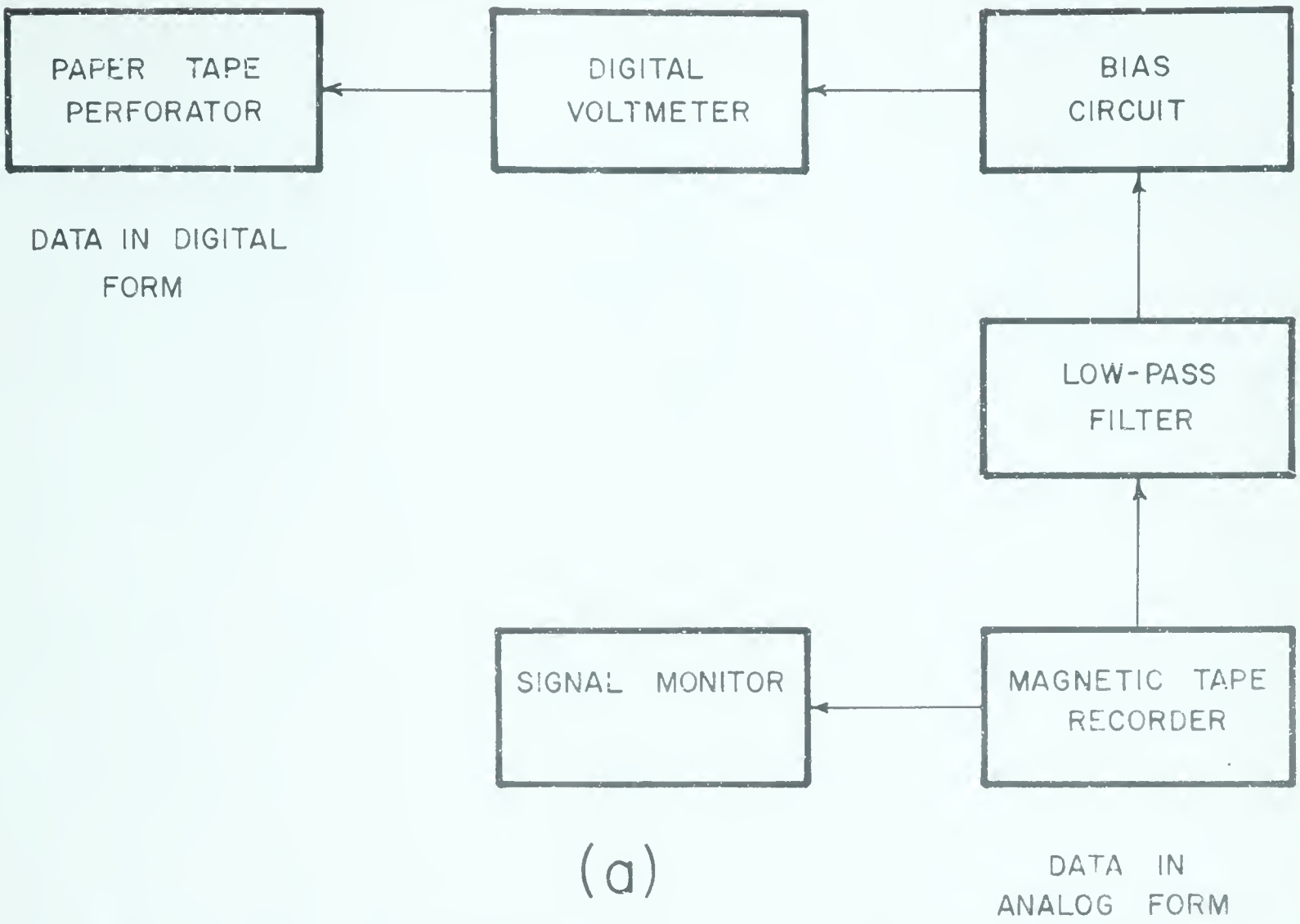

(a)

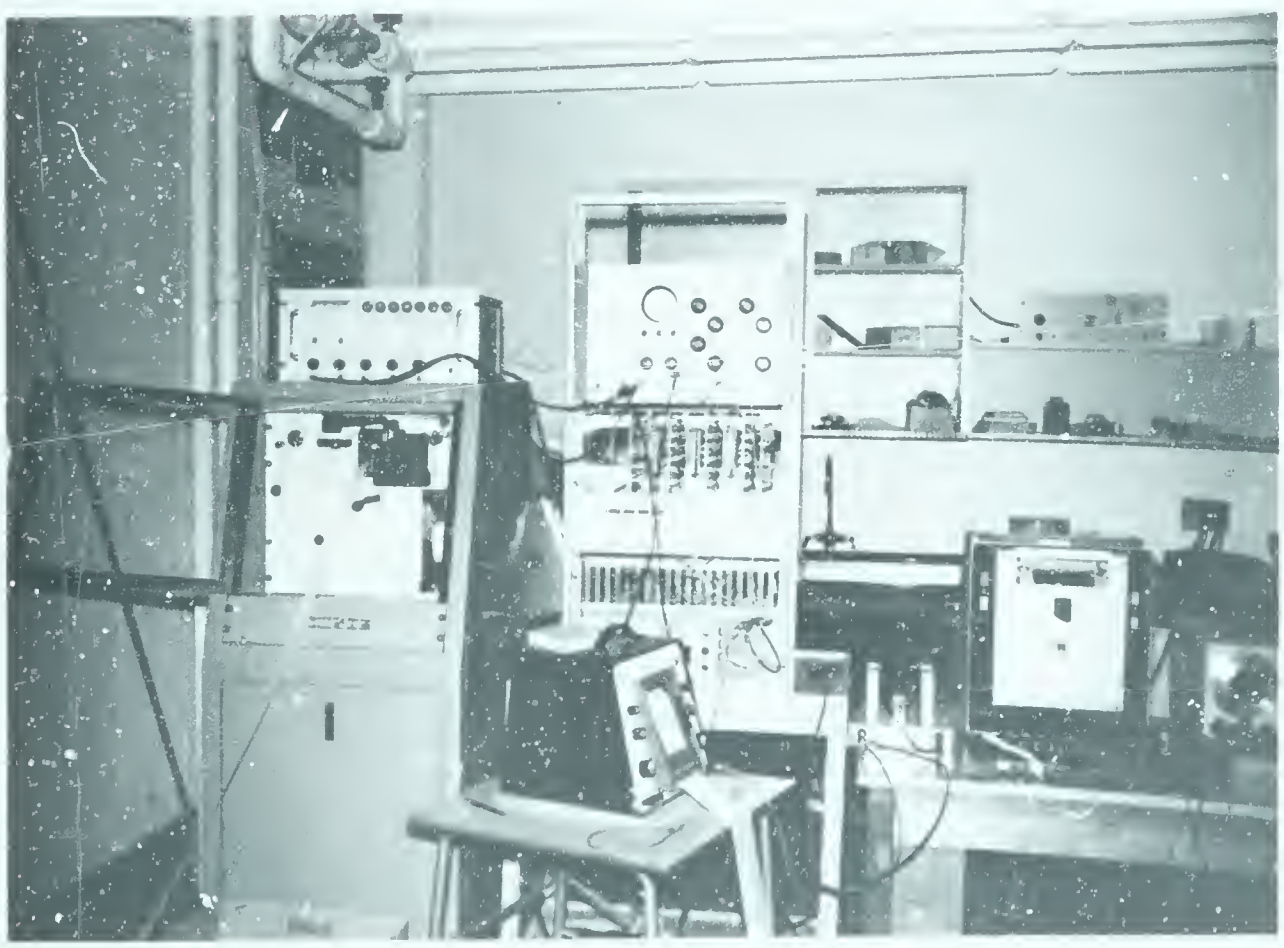

(b)

Fig. 11. Block diagram (a) and photograph (b) of PLAYBACK CIRCUIT.

frequency component of approximately 0.5 cps. In Figure 13, which is a continuation of the preceding record, the paper speed was increased approximately 12 times to enhance the presence of these relatively high frequency components.

The strongest signals recorded were at Cooking Lake. High frequency components can be seen to be superimposed upon much lower frequency components of considerable amplitudes. Figure 15, which is a continuation of Figure 14 but at a paper speed 10 times as high, shows more clearly the presence of these high frequency components. The records taken at this station yielded useful information over a wider frequency range than those taken at the other four stations.

In Figure 16 is shown a section of the record taken at Irricana. At this location, the depth to the Mohorovicic discontinuity was determined from seismic records (Richard and Walker 1959). It was hoped that magneto-telluric measurements at this site would yield information on subsurface structure down to this seismic discontinuity (43 kilometers). In order to be able to interpret the earth's structure to this depth in central Alberta, periods in the range of 100 to 300 seconds are required. An inspection of the Irricana record shows the longest period present to be of the order of 100 seconds. Subsequent spectral analysis of this record corroborates the above statement.

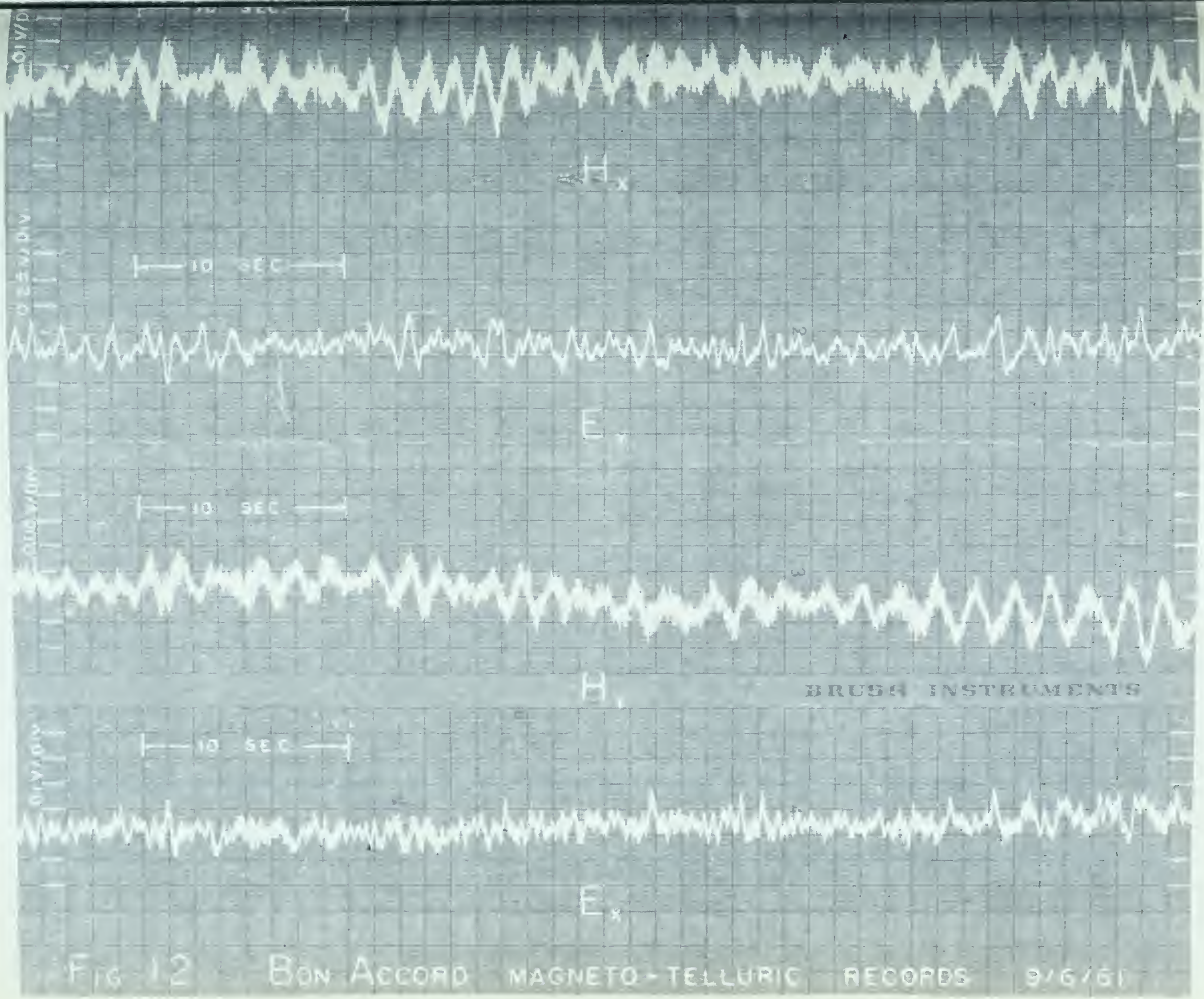

FIG 12 BON ACCORD MAGNETO-TELLURIC RECORDS 9/6/61

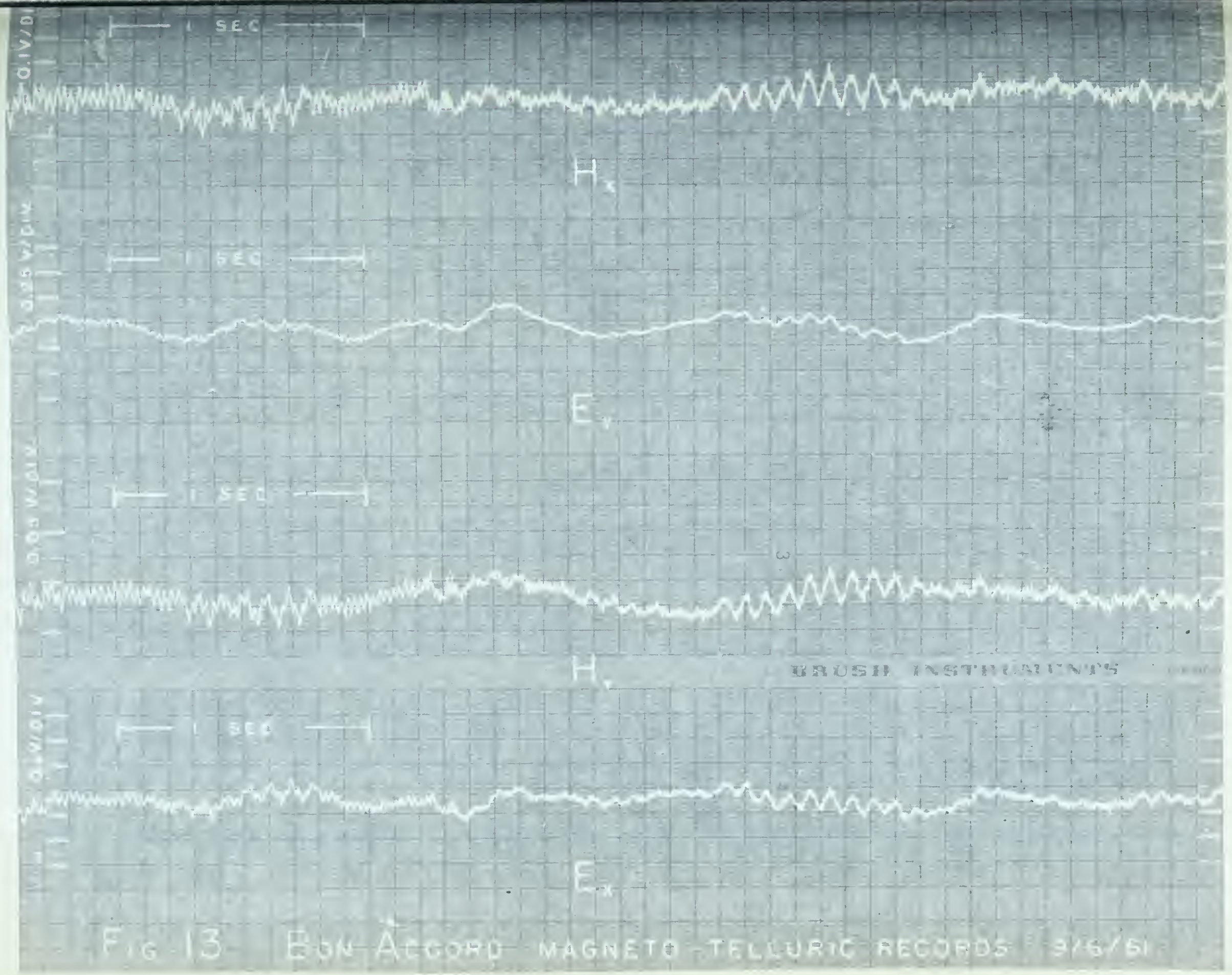

FIG 13 BON ACCORD MAGNETO-TELLURIC RECORDS 9/6/61

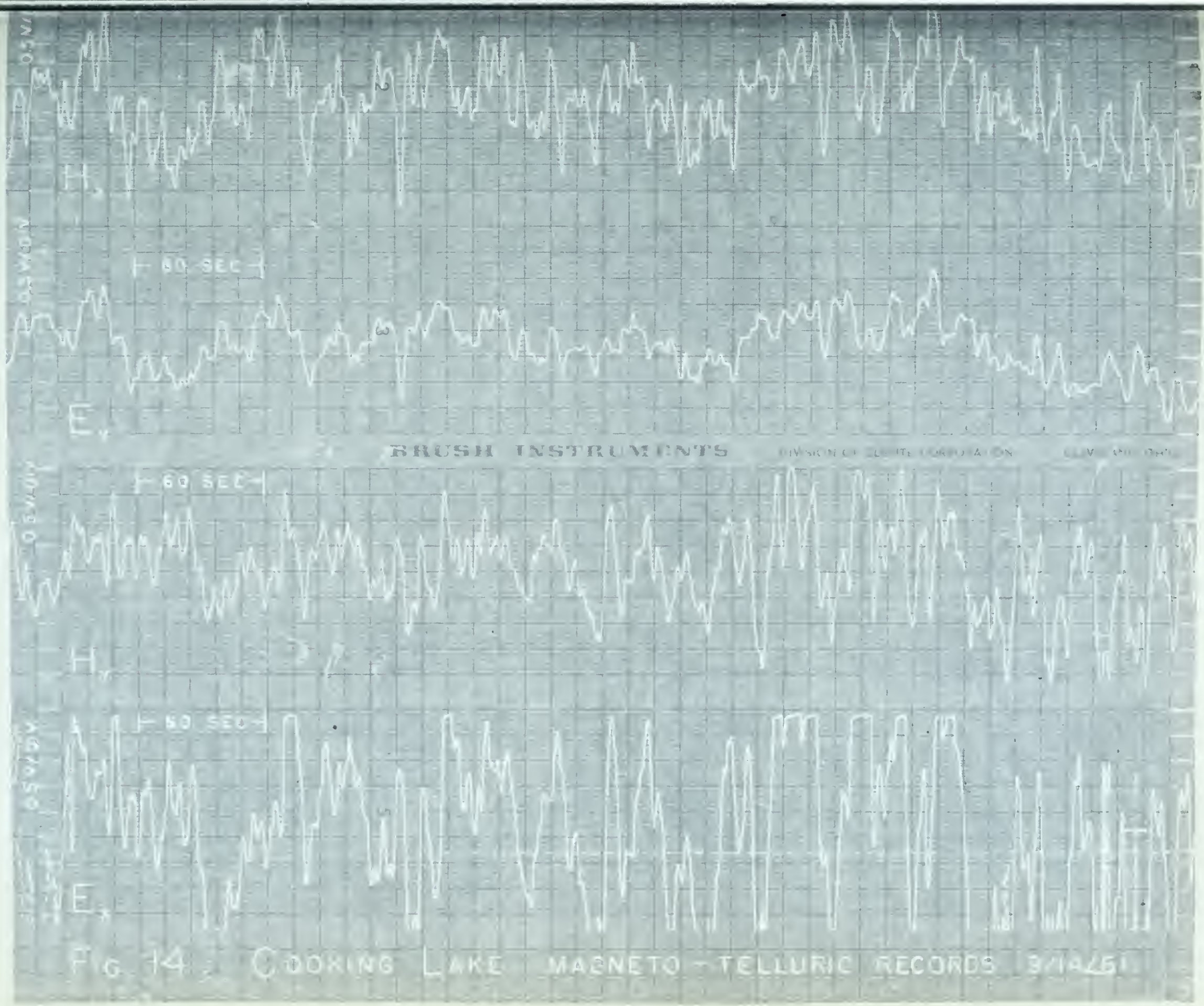

FIG. 14. COOKING LAKE MAGNETO-TELLURIC RECORDS 3/14/51

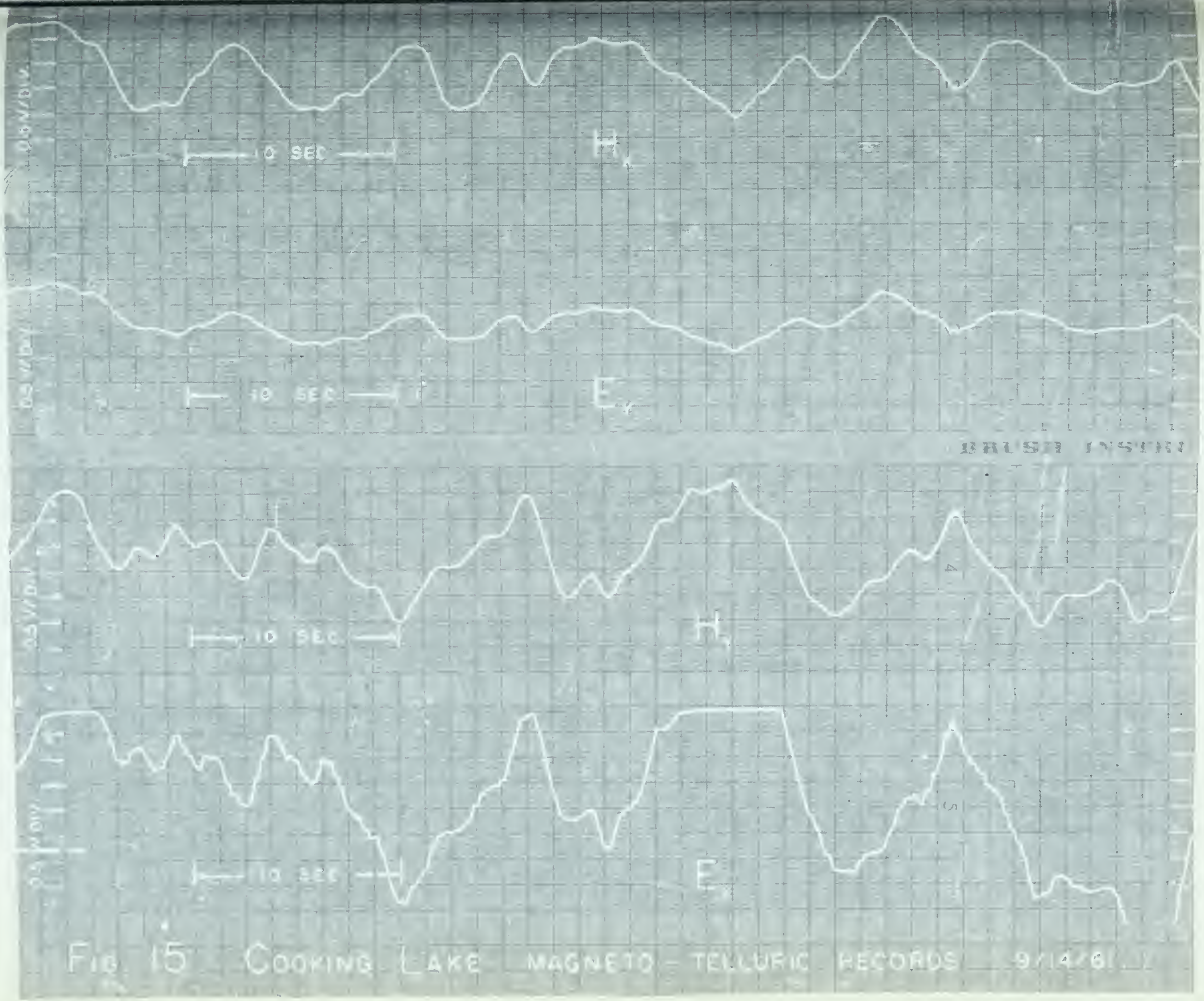

FIG. 15 COOKING LAKE MAGNETO - TELLURIC RECORDS 9/14/61

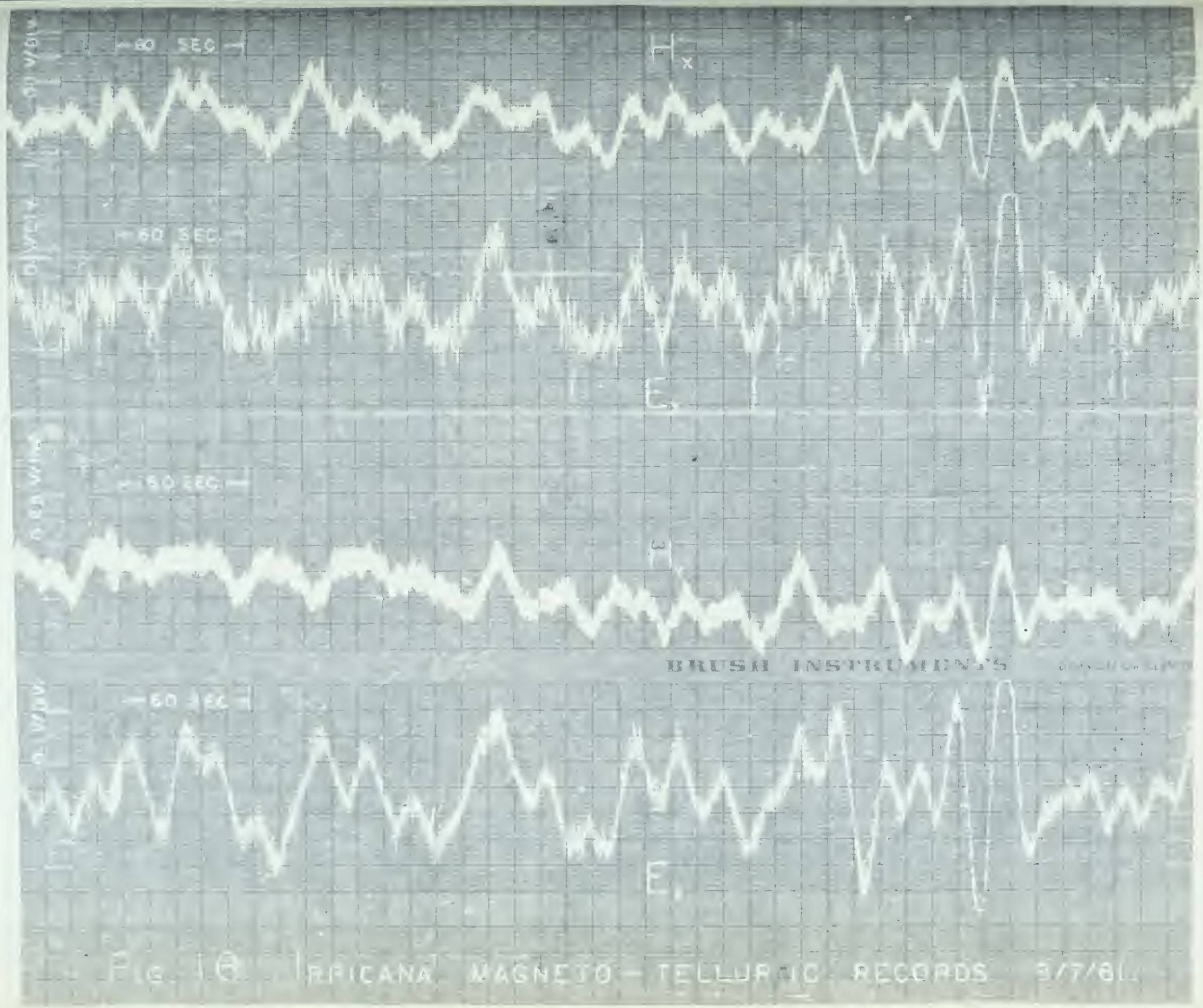

Fig. 16 IRICANA MAGNETO-TELLURIC RECORDS 3/7/81

CHAPTER IV

ANALYSIS OF MAGNETO-TELLURIC DATA

Introduction

Magneto-telluric signals are, in general, a superposition of signals from many different sources. Hence a suitable method for determining the harmonic components which make a significant contribution would be a Fourier analysis. However, because of the noise introduced through the instruments (amplifiers, generator, etc) and external sources (power lines, lightning, etc) a more appropriate method would be one in which much of the noise is eliminated (by statistical means) before the Fourier analysis. Such a method was outlined by Blackman and Tukey, (1958) and was used in this thesis.

Previous methods for analyzing these micropulsations have been the following:

(a) selecting parts of the record where the signal is very nearly sinusoidal and measuring the amplitude and corresponding frequency (Niblett and Sayn-Wittgenstein, 1960).

(b) employing a sufficient number of narrow band-pass filters to cover the frequency range of interest (eg: pass bands at 0.005 - 0.02, 0.02 - 0.06, etc, to 0.6 - 1 cps).

(c) mathematical methods (eg: Statistical Analysis by

Cantwell, 1960).

The latter method was adopted mainly because the data processing could be done entirely by electronic means. Moreover, this method does not require the lengthy record that is required for (a), nor the large number of electronic circuits that is required for (b).

A brief description of the order of data processing is as follows. First, the signal (in analog form) on magnetic tape was converted into digital form by means of the play-back circuit shown in Figure 11. This digitized data (punched on paper tape) was then fed into the IBM 1620. A program was written to calculate first the power spectra (proportional to volts^2) at appropriate frequencies, and second, the apparent resistivities at these frequencies.

Outline of Mathematical Steps

General

Basically, the mathematical operations consist of two steps. The first step consists in determining the auto-covariance $C(\tau)$ at lag τ ; this is a statistical operation. The next step consists in taking the Fourier transform of $C(\tau)$ to obtain the power spectrum $P(f)$; the latter is proportional to the square of the amplitude at frequency f. Expressions for the above two quantities are given for the case of a continuous, infinitely long record. Modifications to these expressions are then made when the record is of

finite duration and in digital form. No derivations will be given.

Continuous, Infinite Record

Expressions for $C(\tau)$ and P(f) for the case of a continuous, infinitely long record will be given. Suppose X(t) is the voltage between two points on the earth's surface. The autocovariance at lag τ is then defined as:

$$C(\tau) = \text{ave}\left[X(t+\tau) . \bar{X}(t) \right]$$

$$= \lim_{T \to \infty} \frac{1}{2T} \int_{-T}^{T} X(t+\tau) . \bar{X}(t)\, dt \quad . \quad . \quad . \quad . \text{IV - 1}$$

where the bar denotes complex conjugacy. In this case X(t) is real and the bar may be omitted. When $\tau = 0$, C(0) is called the variance and is given by:

$$C(0) = \lim_{T \to \infty} \frac{1}{2T} \int_{-T}^{T} X(t) . \bar{X}(t)\, dt \quad . \quad . \quad . \quad . \text{IV -2}$$

Inspection of IV - 2 shows that, if the resistance between the electrodes be taken as 1 ohm, then C(0) is a measure of power. In fact, C(0) represents the average amount of power dissipated per unit time, that is the sum of the powers of all the component frequencies. Hence $C(\tau)$ may be written as:

$$C(\tau) = \int_{-\infty}^{\infty} P(f) . e^{i 2\pi f \tau}\, df \quad , \quad . \quad . \quad . \quad . \text{IV - 3}$$

where P(f) is referred to as the spectral density or

simply the power spectrum. The Fourier transform of IV - 3 is:

$$P(f) = \int_{-\infty}^{\infty} C(\tau) . e^{-i2\pi f\tau} d\tau \quad \ldots\ldots \text{IV - 4}$$

An alternative expression for P(f) is, using IV - 3 and IV - 4:

$$P(f) = \lim_{T\to\infty} \frac{1}{2T} \left| \int_{-T}^{T} X(t) . e^{-2\pi i f t} dt \right|^2 . \quad \ldots\ldots \text{IV - 5}$$

The power spectrum curve with suitable modifications, usually has a reasonably simple shape which represents fairly accurately the actual physical situation (Blackman and Tukey, page 88).

When the unmodified or raw power spectrum is calculated from IV - 5, the resulting graph has a very irregular fine structure that has little in common with the actual physical situation (H. P. F. Swinnerton-Dyer, (1962). In order to avoid this undesirable situation, the refined power spectrum can be calculated by using IV - 1 and IV - 4 together with a "smoothing function". Hence a smoothed power spectrum can be calculated directly.

Finite Record

Modifications to the above expressions become necessary when the records are taken over a finite time interval, T_n say. $C(\tau)$ must then equal zero when $|\tau| > T_n$. A function

which performs this operation and which also acts as a smoothing function is the following:

$$G(\tau) = \tfrac{1}{2}\left(1 + \cos\frac{\pi\tau}{T_m}\right) \qquad |\tau| < T_m < T_n.$$

$$= 0. \qquad |\tau| \geq T_m. \qquad \ldots .IV - 6$$

This function was used in the determination of P(f) in this thesis.

Digitized Record

Digitization of the data introduces an effect called "aliasing". The effect of the latter is to limit the upper frequency at which reliable values for P(f) are obtainable. Suppose readings of the amplitude of a magneto-telluric signal are taken at uniformly spaced intervals $t = 0, \Delta t, \ldots n\Delta t$. Then aliasing is said to occur at frequency f_1, when $P(f_1)$ represents not just the power at this frequency, but in addition, the sum of the powers at $f_1 \pm \frac{1}{\Delta t}$, $f_1 \pm \frac{2}{\Delta t}$, etc. In order to ensure that this situation does not occur, an upper frequency limit, f_N say, must be selected so that all the desired information is contained in the frequency range $f < f_N$. This upper-limit frequency is referred to as the "folding" or "Nyquist" frequency and is given by:

$$f_N = \frac{1}{2\Delta t}, \qquad \ldots .IV - 9$$

where Δt is the time interval between readings.

Since the signal response of the amplifying circuits was poor above 1 cps, an appropriate value for Δt would be $\frac{1}{2}$ second, so that $f_N = 1$ cps. Thus P(f) can, in principle, be obtained for frequencies less than 1 cps.

Once a value for Δt is selected, then the power spectrum can be calculated at equi-spaced points at frequencies:

$$f_i = \frac{i}{2 m \Delta t} \qquad i = 0, 1, 2, \ldots m \qquad \ldots .IV - 10$$

where m is the number of lags. The larger m is, the greater the detail that appears in the power spectrum curve; however, this detail becomes less reliable. An upper limit on m is that it must be much less than n, the total number of readings.

Procedure for determining power spectrum from a digitized record of uniform spacing of finite length is as follows:

(1) evaluate the mean lagged products with lag interval $\Delta\tau = h\Delta t$ by using:

$$C_r = \frac{1}{n - hr} \sum_{q=0}^{q=n-hr} X_q \cdot X_{q+hr} \qquad \ldots .IV - 11$$

$$\left(r = 0, 1, \ldots m, \text{ where } m \leqq \frac{n}{h} \right)$$

(2) evaluate raw power spectrum (volts^2/cps.$2m\Delta t$) from:

$$V_r = \frac{1}{2m} \left[C_0 + 2 \sum_{q=1}^{q=m-1} C_q \cdot \cos \frac{qr\pi}{m} + C_m \cdot \cos r\pi \right] \ldots .IV - 12$$

for r = 0, 1, ...m

(3) evaluate refined power spectrum from:

$$U_r = \frac{1}{4} V_{r-1} + \frac{1}{2} V_r + \frac{1}{4} V_{r+1} \quad \ldots . \text{IV - 13}$$

Power Spectrum Graphs

Graphs of power spectrum (volts^2/cps x 2m Δt) versus frequency were plotted on semi-log paper in Figures 17 to 21. Each figure shows the power for the E component, represented by a solid line, together with the orthogonal H component, represented by a dotted line. The power spectra curves shown are for the amplified signals.

Properties of these graphs common to most of these curves are the sharp peak in the 0.01 to 0.03 cps frequency range and the steep slopes in both directions from this peak. At frequencies above 0.2 cps, most of these curves show a very jagged fine structure which is the result of noise (mainly from the electronic equipment but also from the signal). The power in this frequency range is, in general, so small as to be masked completely by this noise. The noise level of the electric component (with these amplifiers) is generally greater than the corresponding magnetic noise level by a factor of 10 (see Figure 17b).

Most graphs show a good correlation between the electric and corresponding orthogonal magnetic component.

The only curves which show an increase in power as

the frequency increases from 0.2 cps are the Bon Accord curves. A second maximum point in those curves occur at about 0.52 cps.

The curves which show the least drop-off in power from the main peak at 0.02 cps are the Cooking Lake power spectra. These curves are the only ones which yield reliable information in the frequency range 0.2 to 0.5 cps.

The Irricana power spectra shows a sharp drop-off in power as the frequency decreases from 0.03 cps. Consequently an interpretation at great depths was not possible because of this absence of power at long periods.

Since the maximum frequency at which useful information is obtainable from these power spectra is approximately 0.5 cps or a period of 2 seconds, the shallowest depth at which subsurface structure can be interpreted from these curves is 2 kms (skin depth $p = \frac{1}{2\pi}\sqrt{10\rho T}$ km). This value can be obtained from Table 1 when the surface resistivity is taken as 10 ohm meters and the period, 2 seconds. In central Alberta, the resistivity of the surface layer is just under 10 ohm meters.

BON ACCORD

POWER SPECTRA

NO. OF READINGS n = 6948
NO. OF LAGS m = 100
FOLDING FREQ. f_N = 1/2Δt
= 1.00

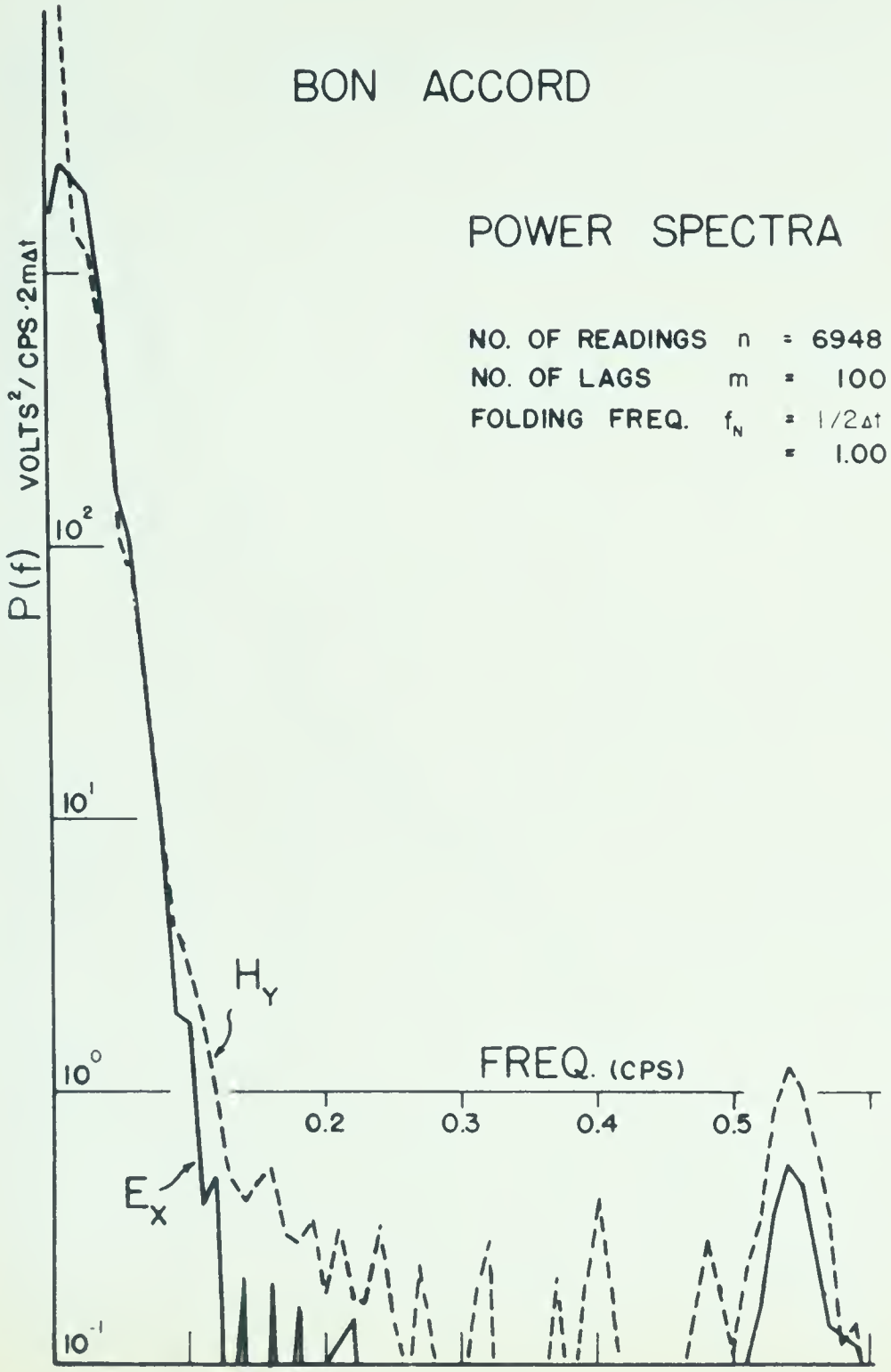

Fig. 17(a)

BON ACCORD

POWER SPECTRA

NO. OF READINGS n = 6948
NO. OF LAGS m = 100
FOLDING FREQ. f_N = 1/2Δt
= 1.00

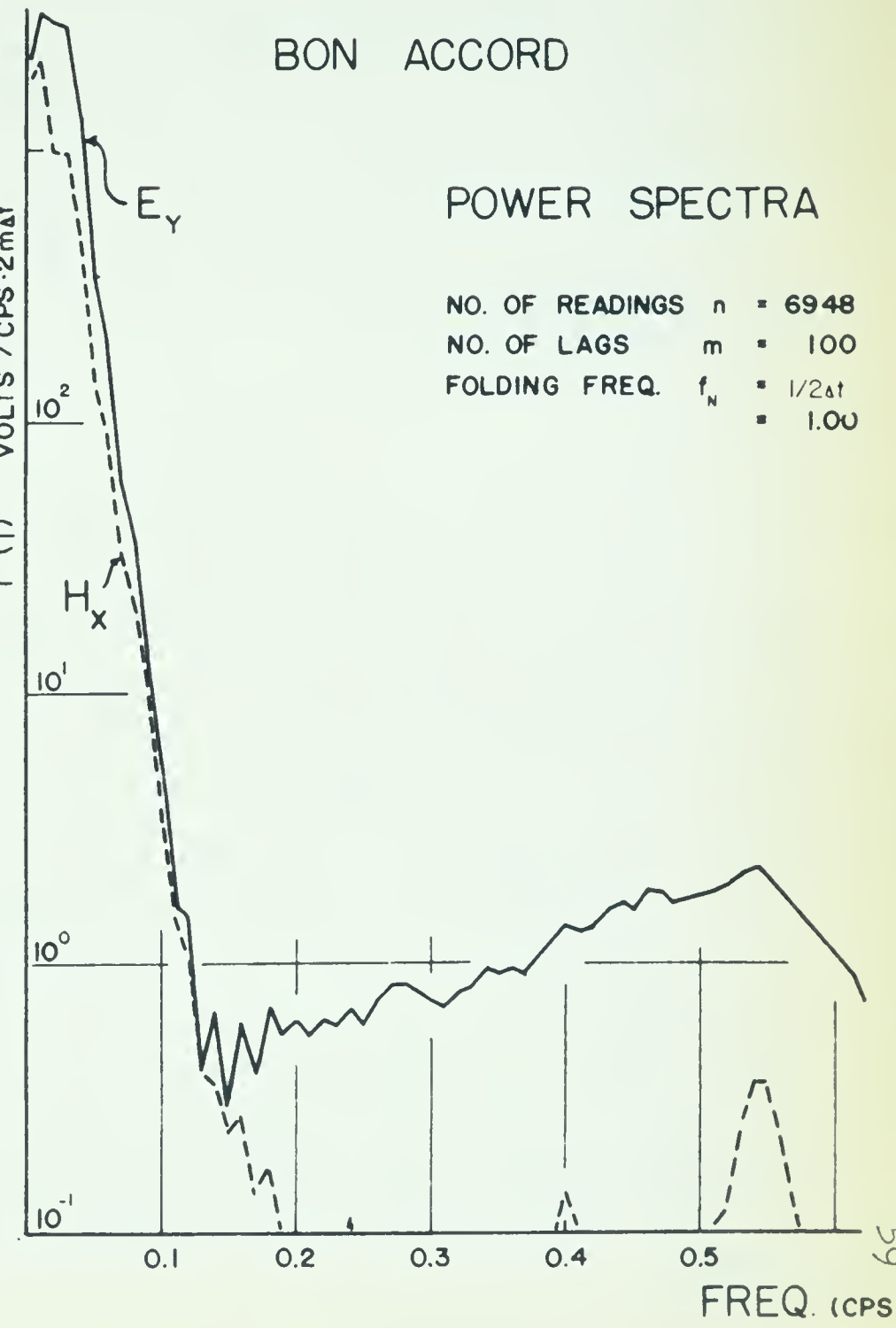

Fig. 17(b)

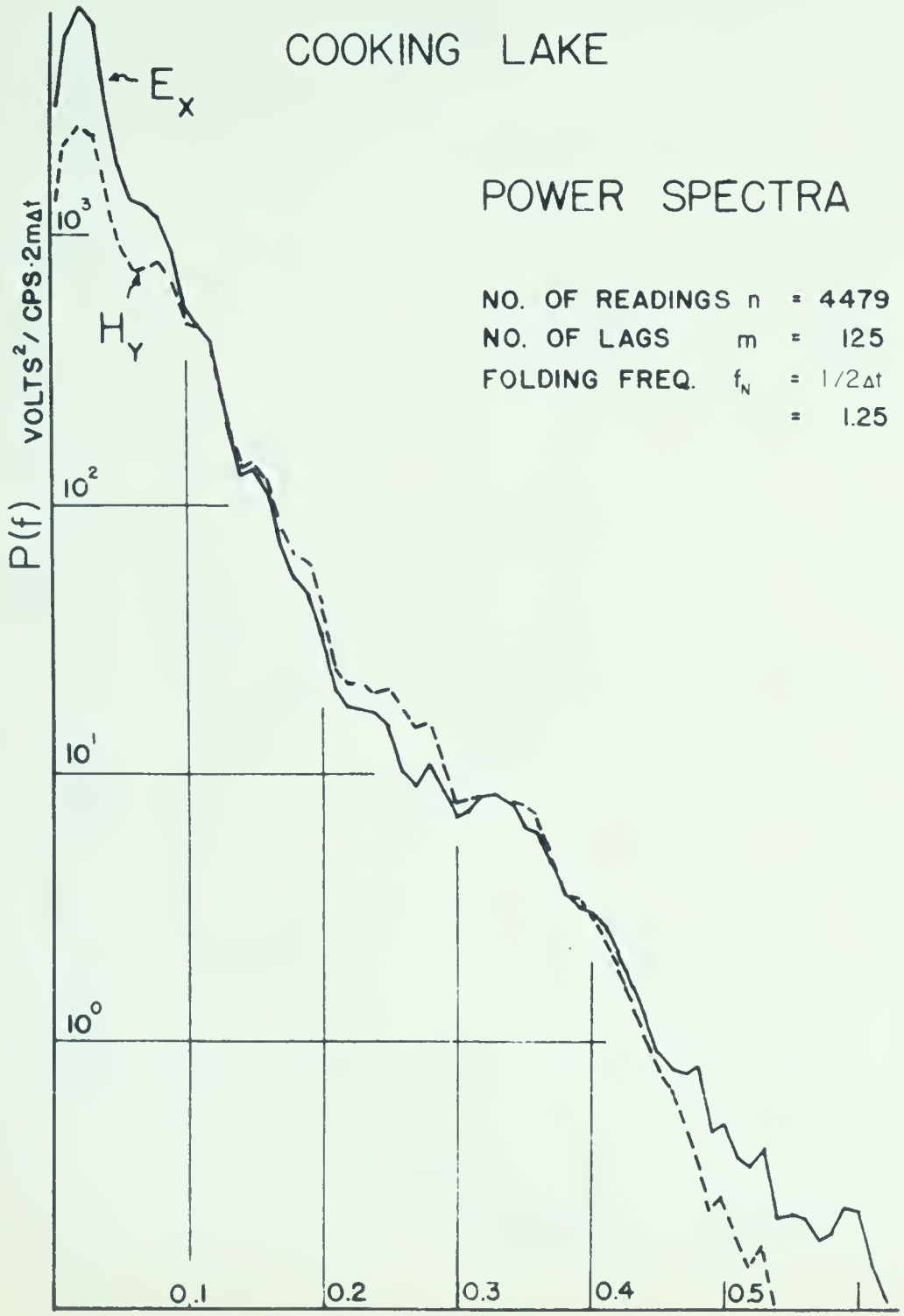

Fig. 13(a)

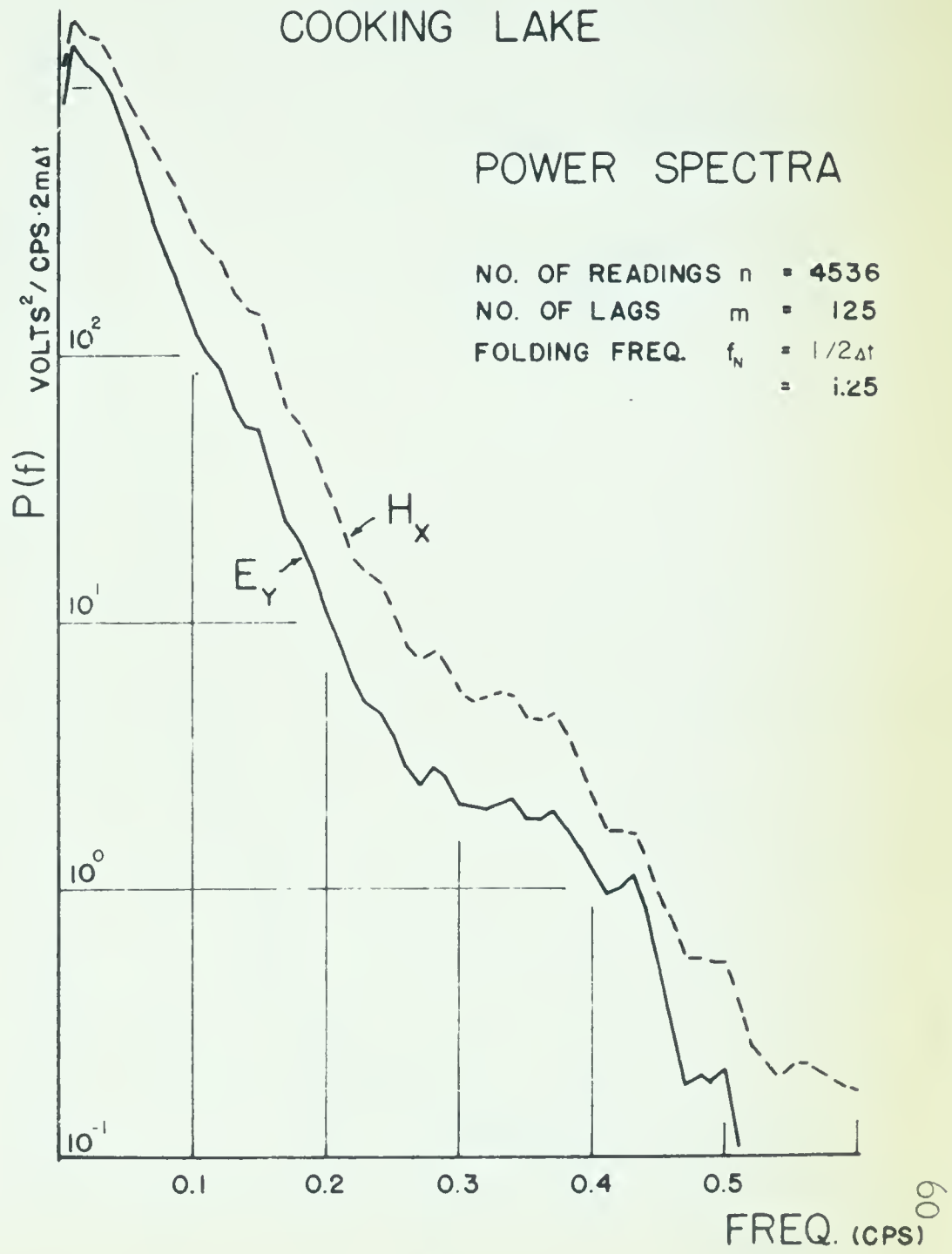

Fig. 13(b)

ONOWAY

POWER SPECTRA

NO. OF READINGS n = 6672
NO. OF LAGS m = 100
FOLDING FREQ. f_N = 1/2Δt
= 1.00

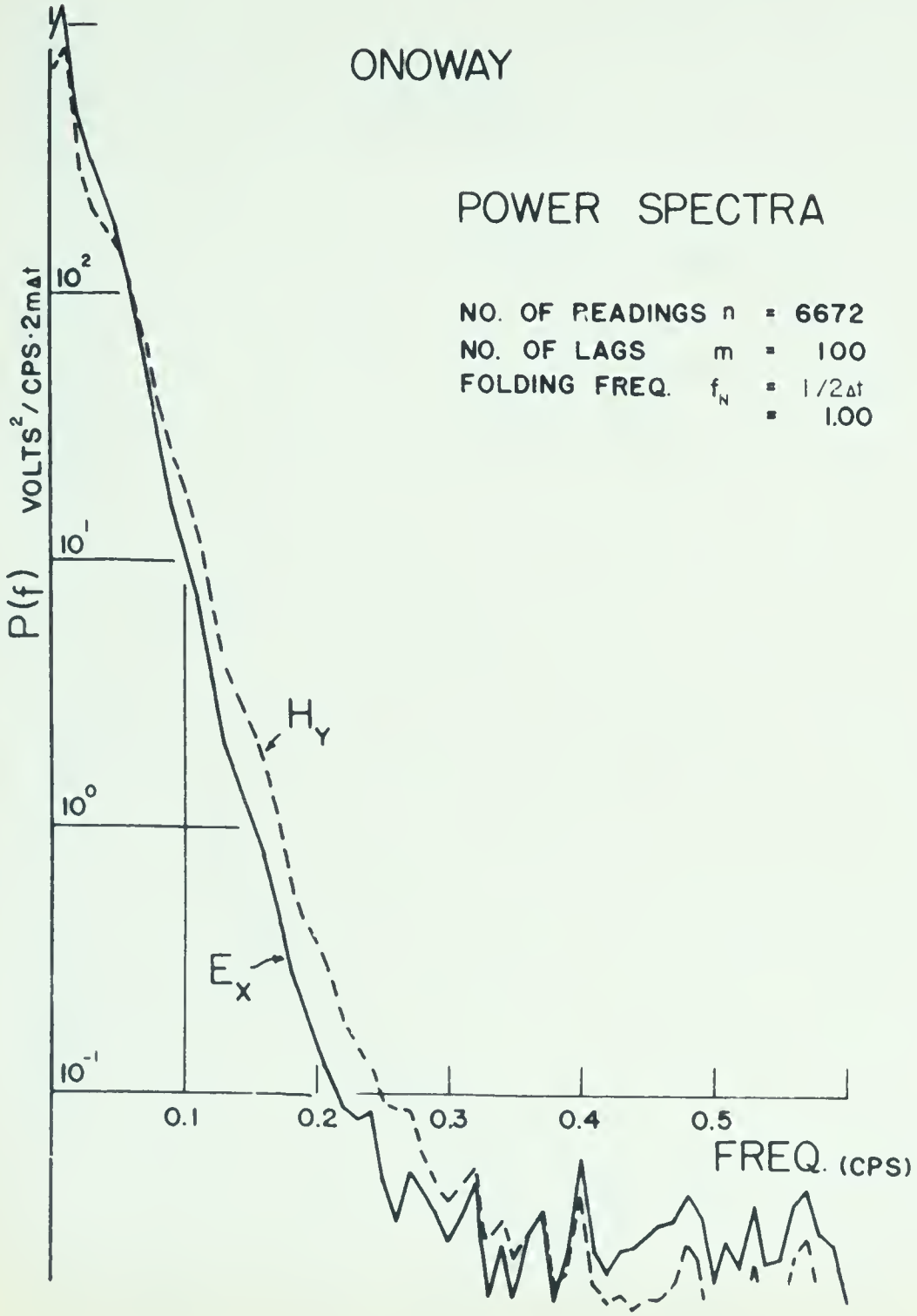

Fig. 19(a)

ONOWAY

POWER SPECTRA

NO. OF READINGS n = 6660
NO. OF LAGS m = 100
FOLDING FREQ. f_N = 1/2Δt
= 1.00

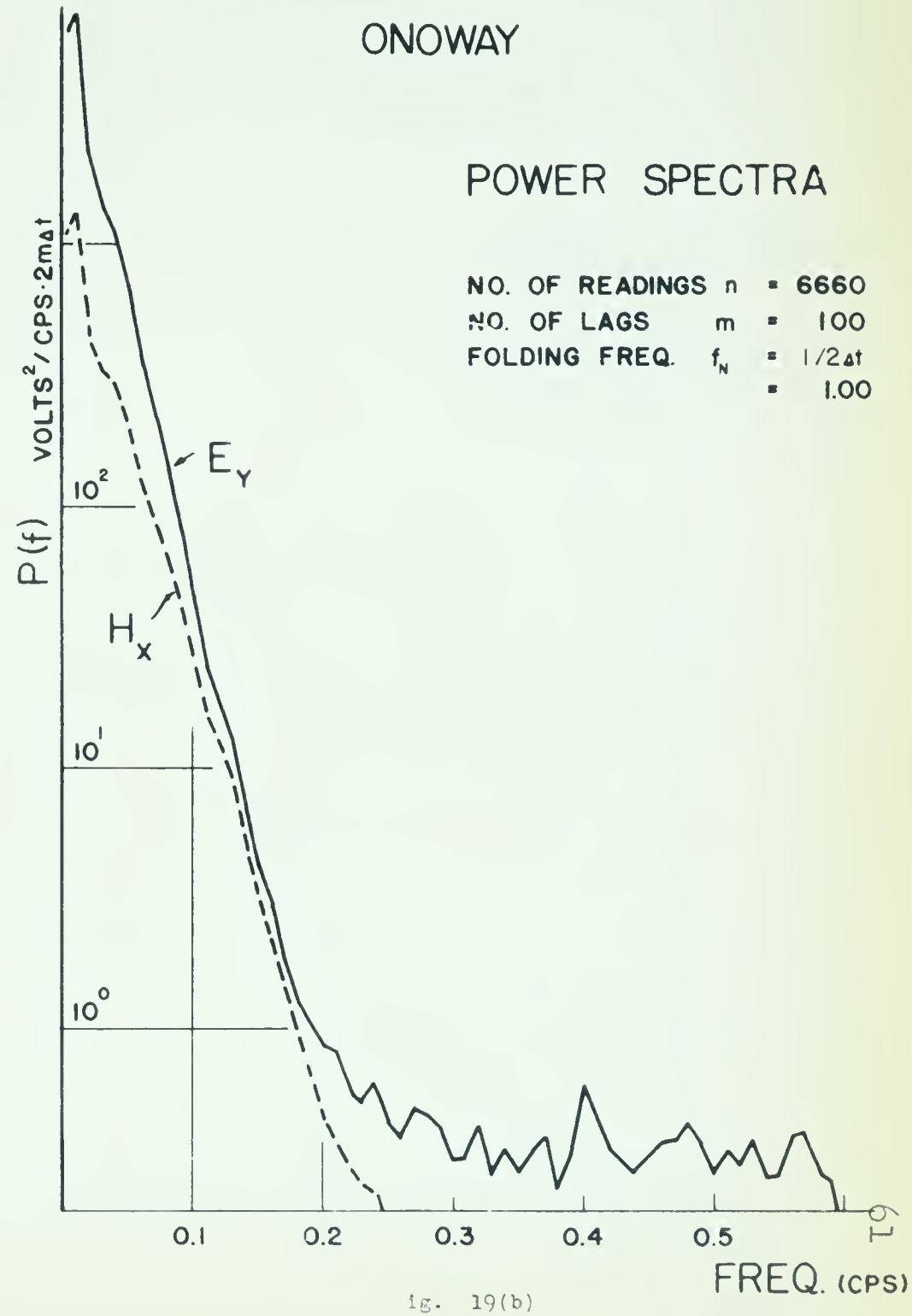

Fig. 19(b)

KAVANAGH

POWER SPECTRA

NO. OF READINGS n = 5328
NO. OF LAGS m = 100
FOLDING FREQ. f_N = 1/2Δt
= 1.00

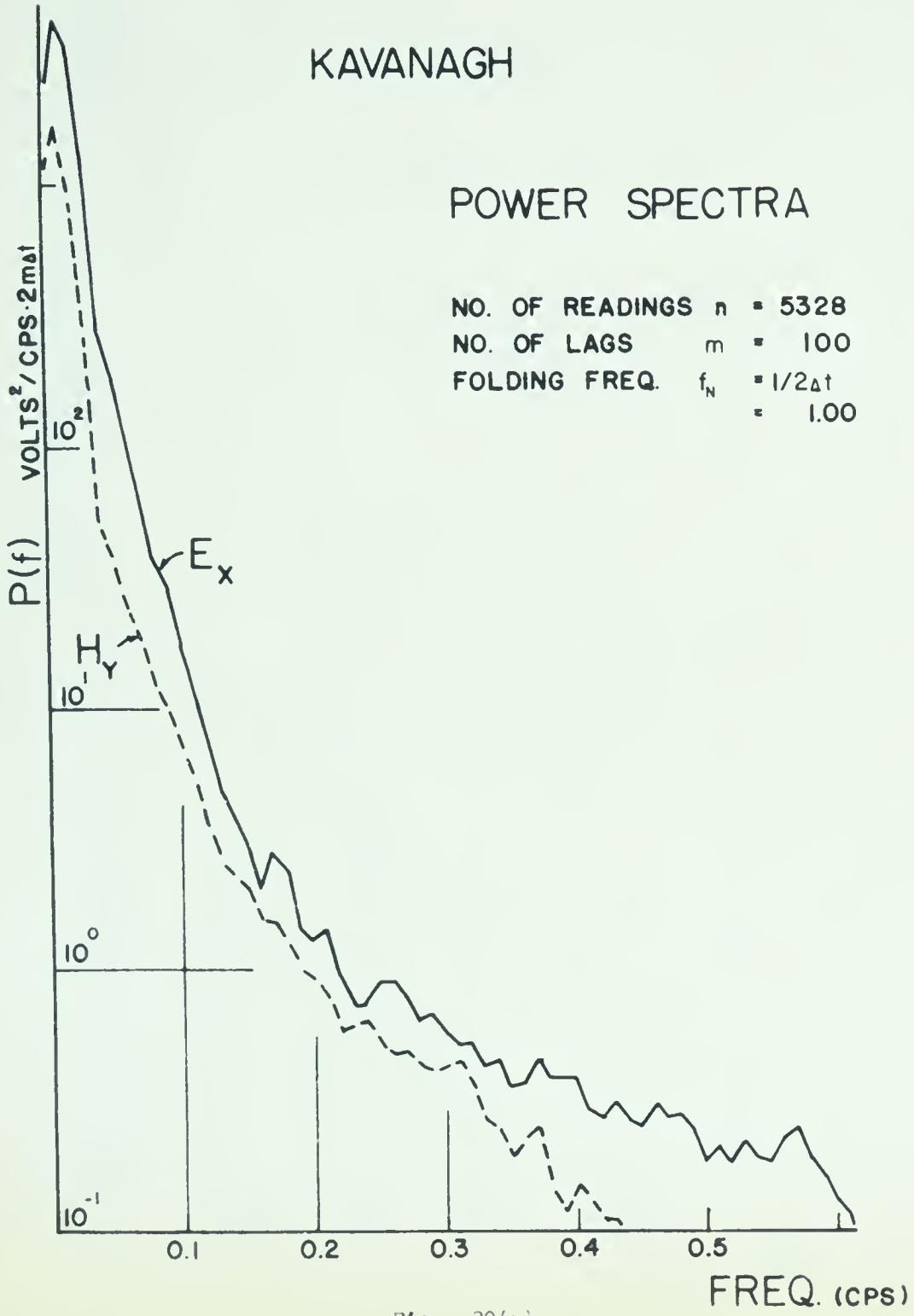

Fig. 20(a)

KAVANAGH

POWER SPECTRA

NO. OF READINGS n = 5328
NO. OF LAGS m = 100
FOLDING FREQ. f_N = 1/2Δt
= 1.00

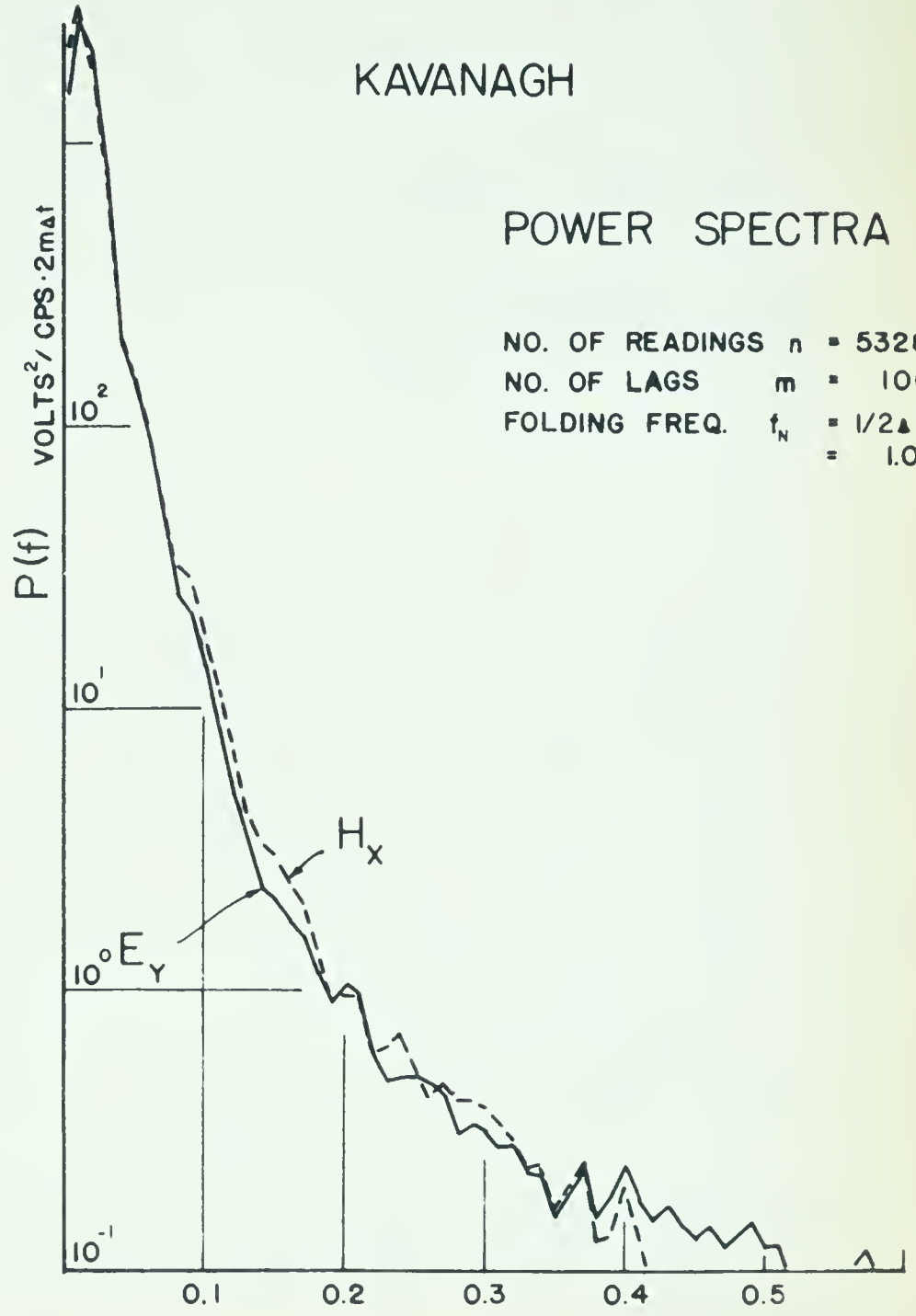

Fig. 20(b)

IRRICANA

POWER SPECTRA

NO. OF READINGS n = 3987
NO. OF LAGS m = 300
FOLDING FREQ. f_N = 1/2Δt
= 1.00

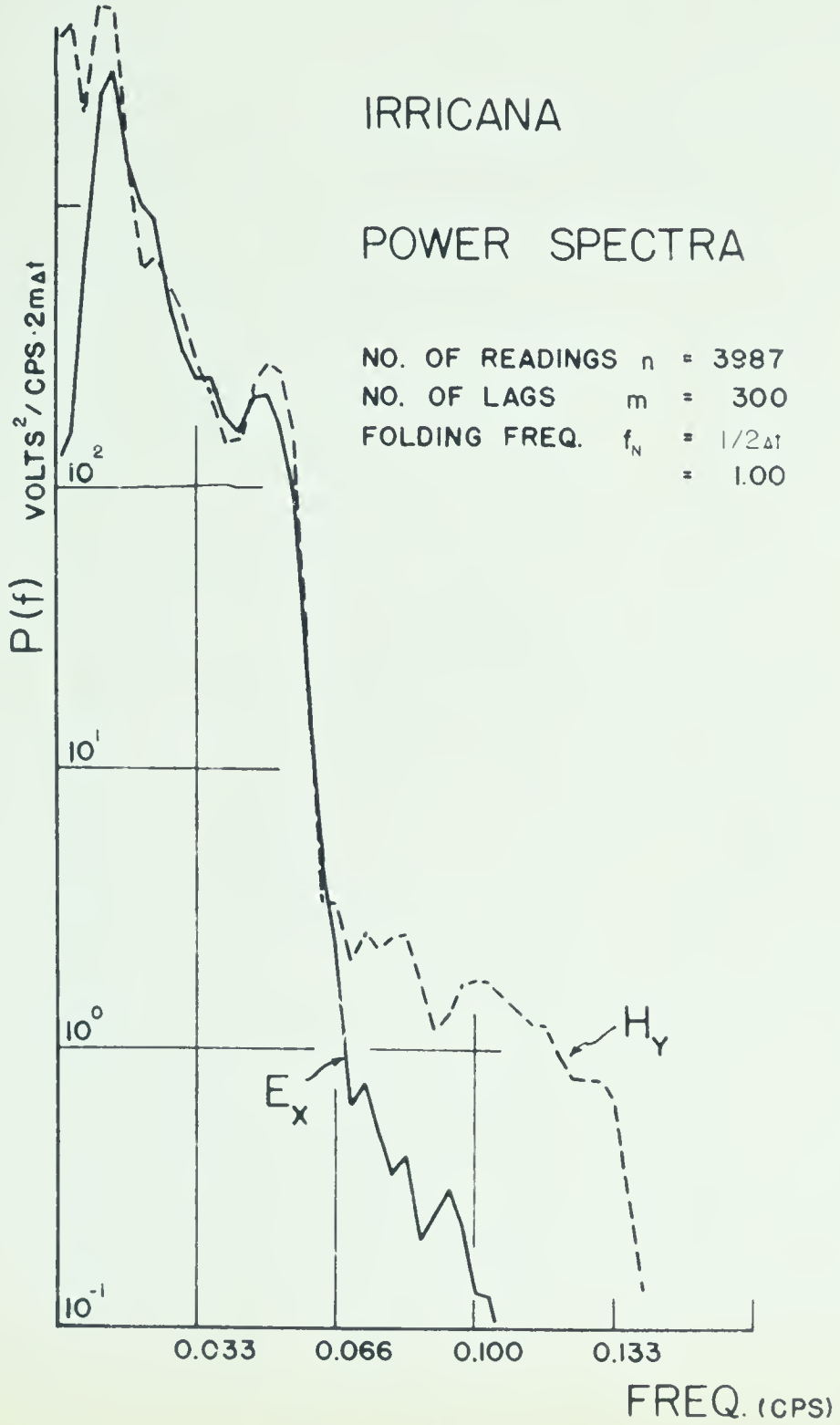

Fig. 21(a)

IRRICANA

POWER SPECTRA

NO. OF READINGS n = 3987
NO. OF LAGS m = 300
FOLDING FREQ. f_N = 1/2Δt
= 1.00

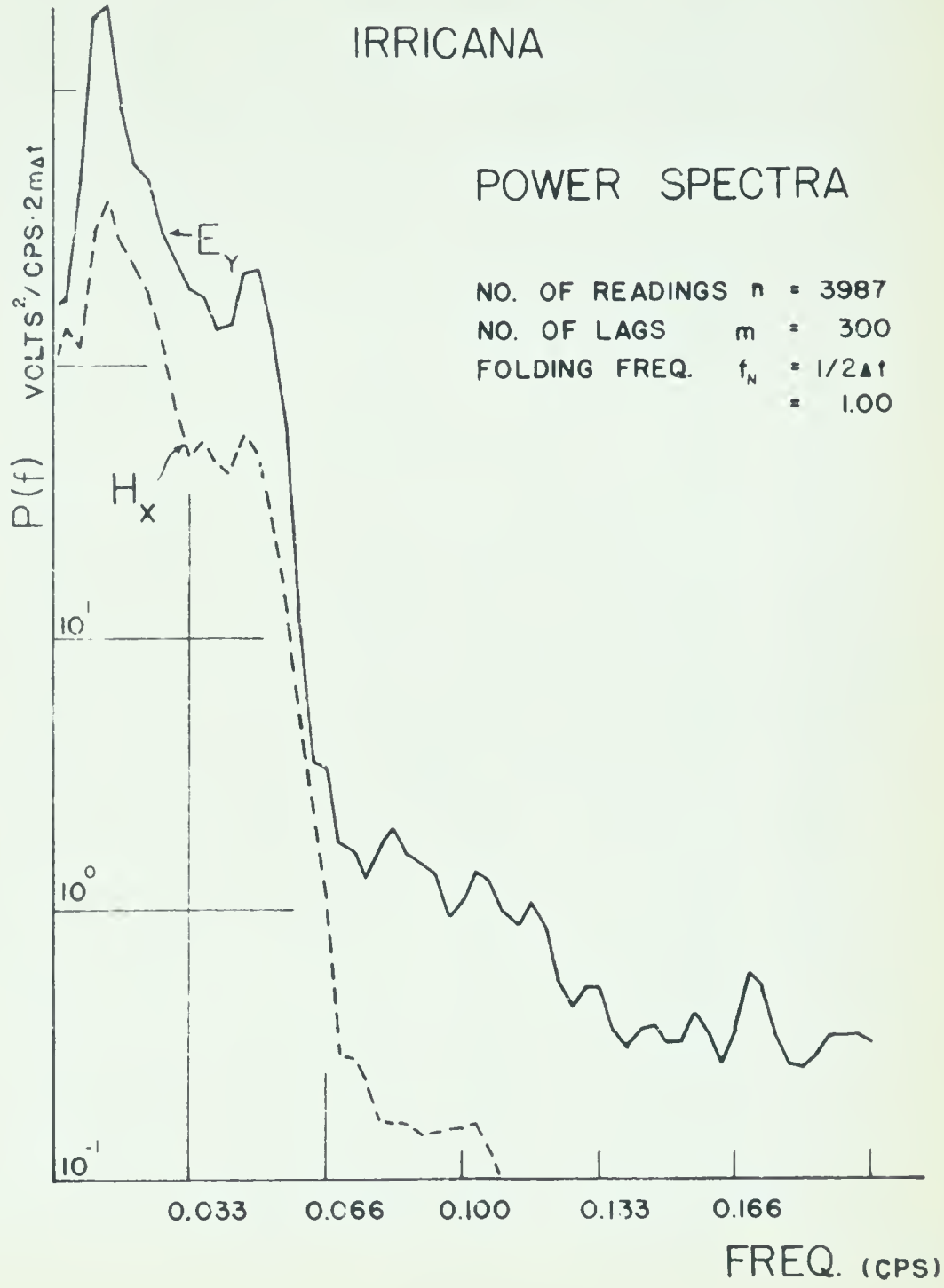

Fig. 21(b)

CHAPTER V

RESULTS AND INTERPRETATION

Calculation of Experimental Resistivity (in practical units)

The electric field intensity, say E_x, between electrodes with a separation of d(ft) is given by:

$$E_x = \left(\frac{1}{d(ft) \times 0.3084 \frac{Km}{ft.}}\right)\left(\frac{1}{\text{Amplification of } E \frac{V_{out}}{mV_{in}}}\right)(\text{Bias Correction})\left(P(f) \frac{V^2}{cps.2mat}\right)^{1/2}$$

This expression gives E_x in units of millivolts/kilometer. The amplification is obtainable from Figure 10(a); the power, P(f), from Figures 17 to 21.

The corresponding magnetic field, H_y, is given by:

$$H_y = \left(\frac{1}{\text{Amplification of } H \frac{V_{out}}{\gamma_{in}}}\right)(\text{Bias Correction})\left(P(f) \frac{V^2}{cps.2mat}\right)^{1/2}$$

This expression gives H_y in units of gammas.

The apparent resistivity ρ_a is then calculated from:

$$\rho_a = 0.2\, T \left|\frac{E_x}{H_y}\right|^2_{2.0} \quad \text{(in ohm meters)}$$

Experimental Apparent Resistivity Curves

An examination of Figures 23 to 27 show the following features:

(1) low apparent resistivities in the short period range (2 to 10 seconds).

(2) sharp rise in the curves when the period increases from 10 to 100 seconds.

(3) a drop in some of the curves in the region 100 to 300 seconds.

(4) for some locations, corresponding pairs of curves

(E_x,H_y and E_y, H_x) converge as the period becomes shorter.

(5) for some locations, corresponding pairs of curves tend to diverge as the period increases from 10 to 100 seconds.

(6) the period range where useful information is obtainable from a curve correlates very closely to the range where the corresponding power spectrum curve lies above the noise level.

Five-layer Case

These experimental apparent resistivity curves yield no useful information for periods less than 2 seconds; this corresponds to a skin depth of 2 kilometers for central Alberta. Hence an interpretation is not possible for depths shallower than this. Moreover, the shape of the apparent resistivity curves is not known for waves whose periods are less than 2 seconds (that is whose skin depths are less than 2 kilometers). In Figure 22 are shown actual earth models together with corresponding apparent resistivity curves. The data for these models were obtained from electric logs: the locations of the Leduc and Willingdon wells are shown in Figure 3. The resistivities shown for each layer are average values estimated by a visual inspection of the well logs; no attempt was made to obtain the true bed resistivity.

These particular well sites were chosen because their resistivities for the upper Cretaceous are extreme cases;

the maximum resistivity for this layer (as determined from electrical logs) is 8 ohm meters and the minimum, approximately 4 ohm meters. The resistivities for the upper Cretaceous at the 5 recording sites lie in between these values. In addition, the resistivities for the upper Devonian at Leduc and Willingdon are much larger than those at the recording sites. These high resistivities result because of the presence of the highly resistive reefs in the Devonian formation at these two sites.

Consequently, one might expect the experimental apparent resistivity curves to lie in between the Leduc and Willingdon curves in the period range 0.01 to 1 seconds and to lie below the Leduc curve in the period range 1 to 10 seconds.

From this magneto-telluric study, resistivities for the sedimentary basin were obtained which agree with those from electrical logs. The fact that different resistivities for the top layer (of the sedimentary basin) were obtained at different locations is not inconsistent with electrical log values, which are shown in Table III.

For the crystalline basement, the resistivities were found to vary from 600 to 10^6 ohm meters. However, when the value 10^6 is replaced by 10^4 in the theoretical models, there is no appreciable difference in the shape of the corresponding apparent resistivity curve. Hence the resistivity for the Precambrian can be thought of as varying from 600 ohm meters to a very large value, say 10,000 ohm meters. The fact that the resistivity of the Precambrian was found to vary with location is consistent with previous geophysical

and petrological studies of the basement. Electrical logs, from wells in central Alberta which have penetrated into the basement, indicate a sharp rise in resistivity at the lower boundary of the sedimentary basin. Moreover, the logs indicate the resistivity to vary from well to well and vary from 100 to 1,000 ohm meters. However, these are superficial values because the maximum depth of well penetration into the basement is only several hundred feet. Hence the resistivity of the Precambrian as a whole can be expected to be greater than the surface values because the moisture content of the rocks decreases with depth. This is in agreement with the results of this investigation. In addition, the fact that corresponding experimental curves (at given location) tend to diverge is suggestive of an anisotropic crystalline basement.

A rather significant finding is that no electrical discontinuity could be detected at the depth where the Mohorovicic discontinuity is expected to be. This suggests that the Mohorovicic discontinuity, which is a seismic phenomena, cannot be detected by the magneto-telluric method. An electrical discontinuity was detected at a depth of 80 km.

Many of the experimental curves tend to bend over at the long periods, thus indicating the presence of a conducting substratum. However, other factors could produce the same effect. As mentioned in Chapter II, the effect of a source of finite lateral extent is to decrease the apparent resistivity for these long periods. Hence both a finite source as

well as a highly conducting mantle could effect a bend-over of the experimental curve at long periods.

An interesting feature of the Cooking Lake experimental curves is that one curve (E_x, H_y) starts to bend over at a period of 100 seconds, whereas the other (E_y, H_x) does not. A similar situation was observed on the experimental curves obtained at Meanook by Niblett and Sayn-Wittgenstein (1960). However, their (E_x, H_y) curve exhibits this feature at a much longer period (close to 1,000 seconds). A possible explanation of this rather unexpected feature could be a distribution of sources in such a way as to modify only the (E_x, H_y) component of the apparent resistivity at long periods.

Layer of Variable Conductivity

In the interpretations so far, the resistivity for the Precambrian was assumed to be independent of depth. However, the Bon Accord (E_x, H_y) curve (Figure 25) gives indication of a Precambrian with a resistivity which increases with depth. Interpretation by Bossy and DeVuyst (1959) of Belgium of magneto-telluric records taken at Dourbes, indicate that a composite model consisting of a surface layer of constant resistivity overlying a layer in which the resistivity varies continuously with depth seems to represent their experimental results. However, since only one curve gives indication of this feature, no interpretation along the lines of Bossy and DeVuyst was attempted.

TABLE III

APPARENT RESISTIVITY OF THE SEDIMENTARY FORMATIONS OBTAINED FROM ELECTRIC LOGS

PERIOD	FORMATION	Apparent resistivity in ohm meters LEDUC mud res. 2.8Ωm. at 45°F	ARDROSSAN 1.2 Ωm at 60°F	WILLINGDON 1.5Ωm at 64°F
Upper Cretaceous	Edmonton	8	-	-
	Lea Park	7	6	6
Lower Cretaceous	Viking	3	3	3
	Joli Fou	7 - 10	3	3
	Nisku	60 - 300	25	-
Upper Devonian	Ireton	10	6	7
	Reef	50		150
	Beaverhill Lake	30 - 150	15 - 100	10 - 30
Middle Devonian		10 - 30	20 - 50	25 - 50
Upper and Middle Cambrian		10	7 - 13	4 - 15

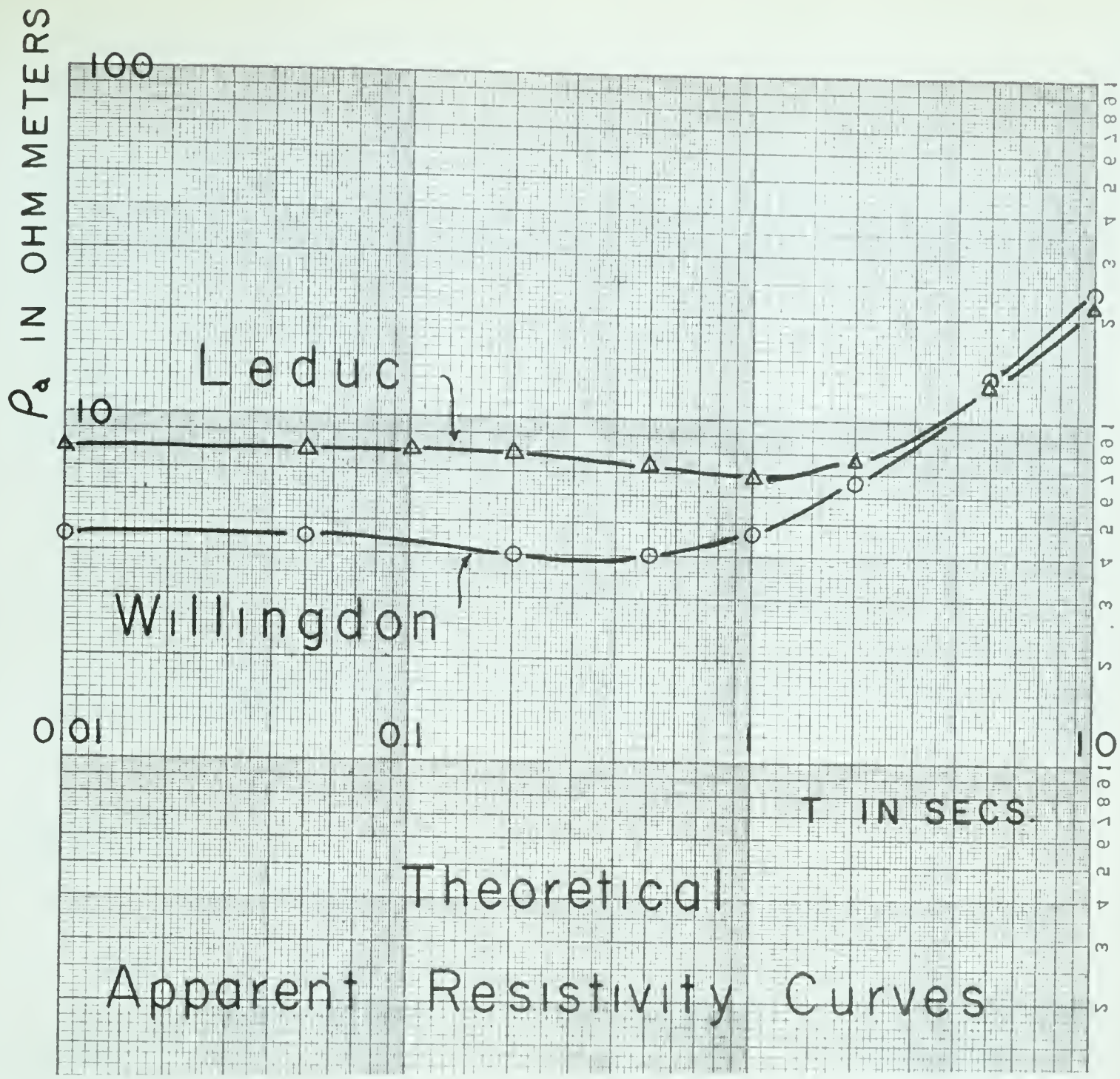

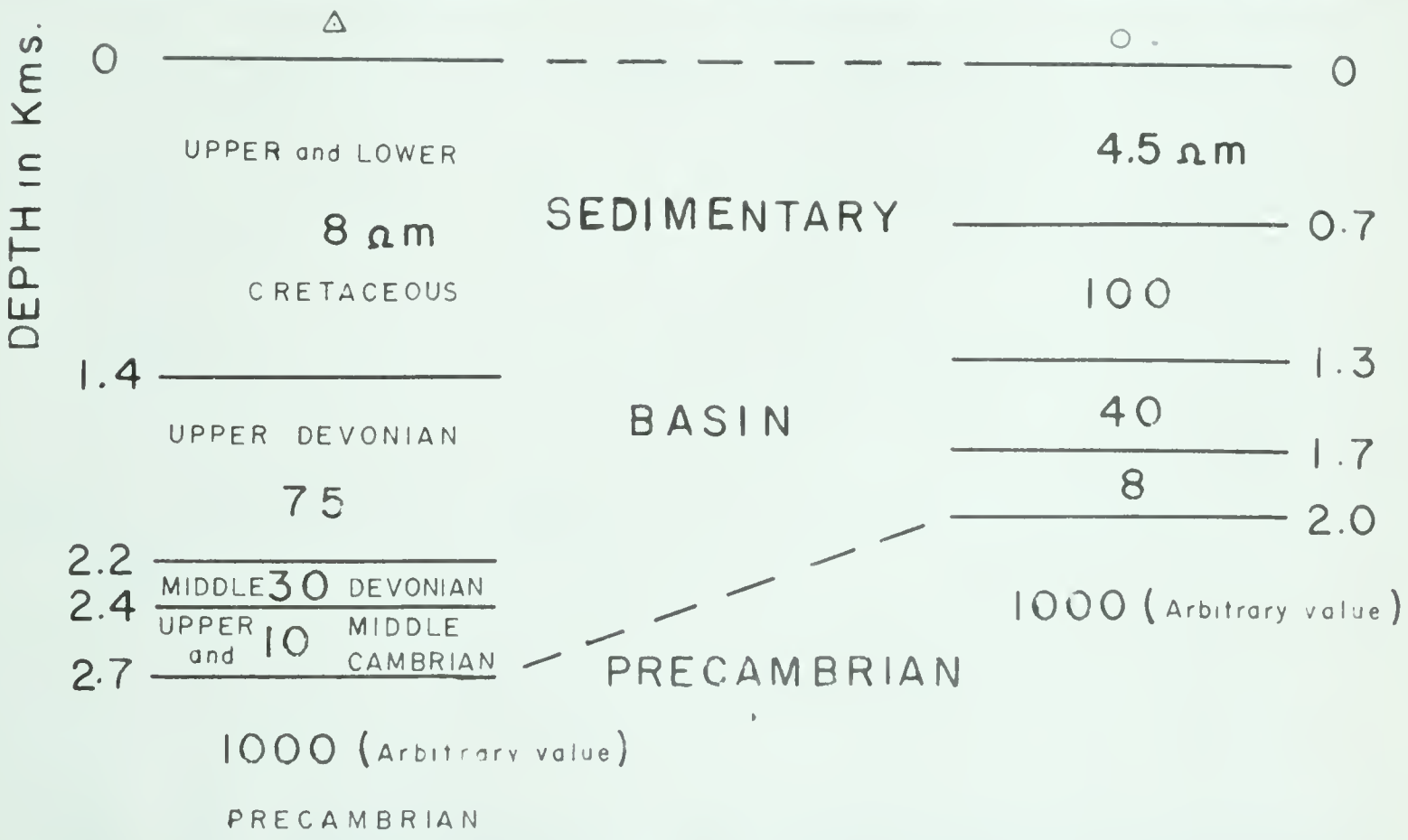

Actual Earth Models

Fig. 22

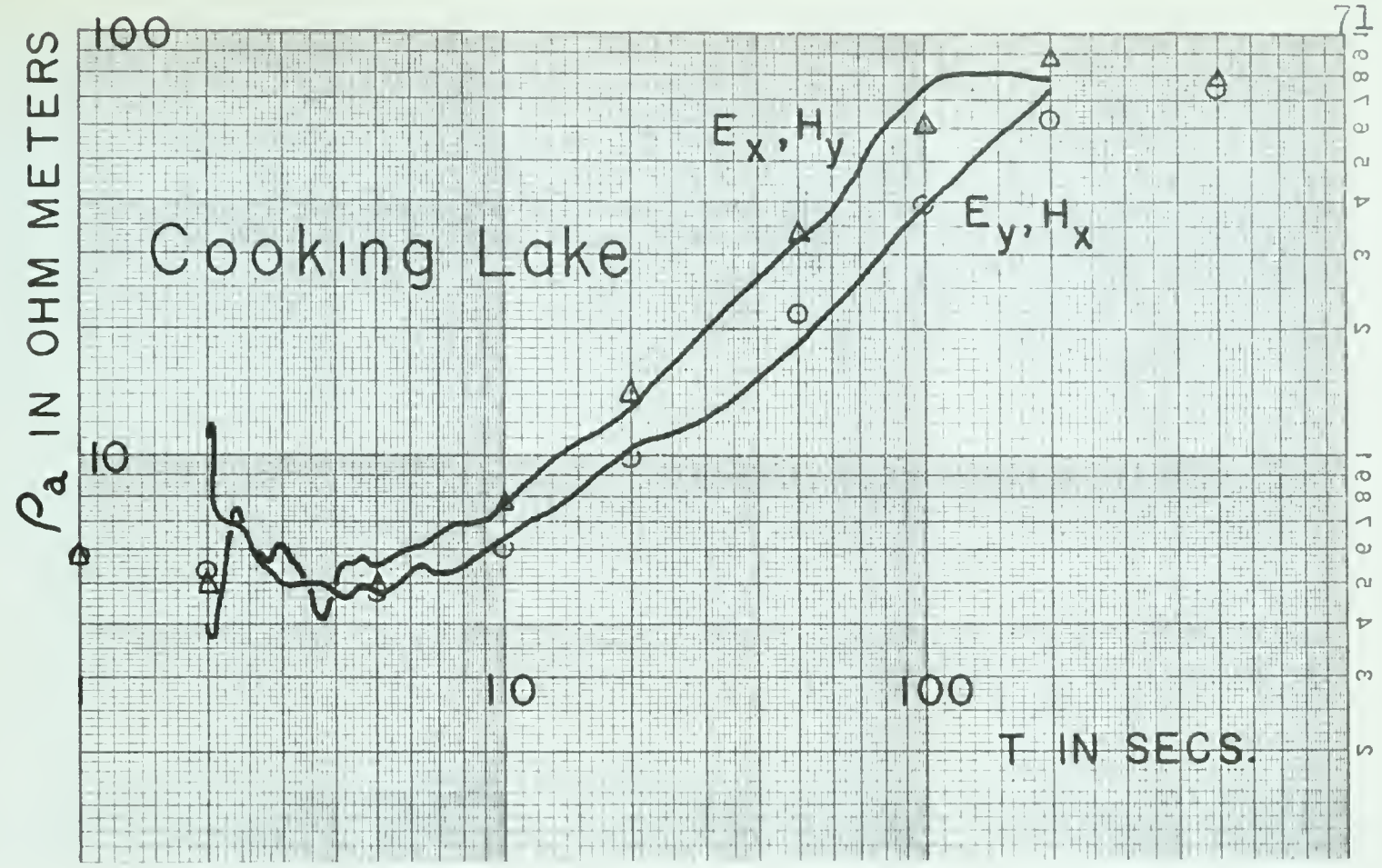

LEGEND

Solid line — Experimental Apparent Resistivity Curves

Δ and ○ — Theoretical Curves and corresponding Models

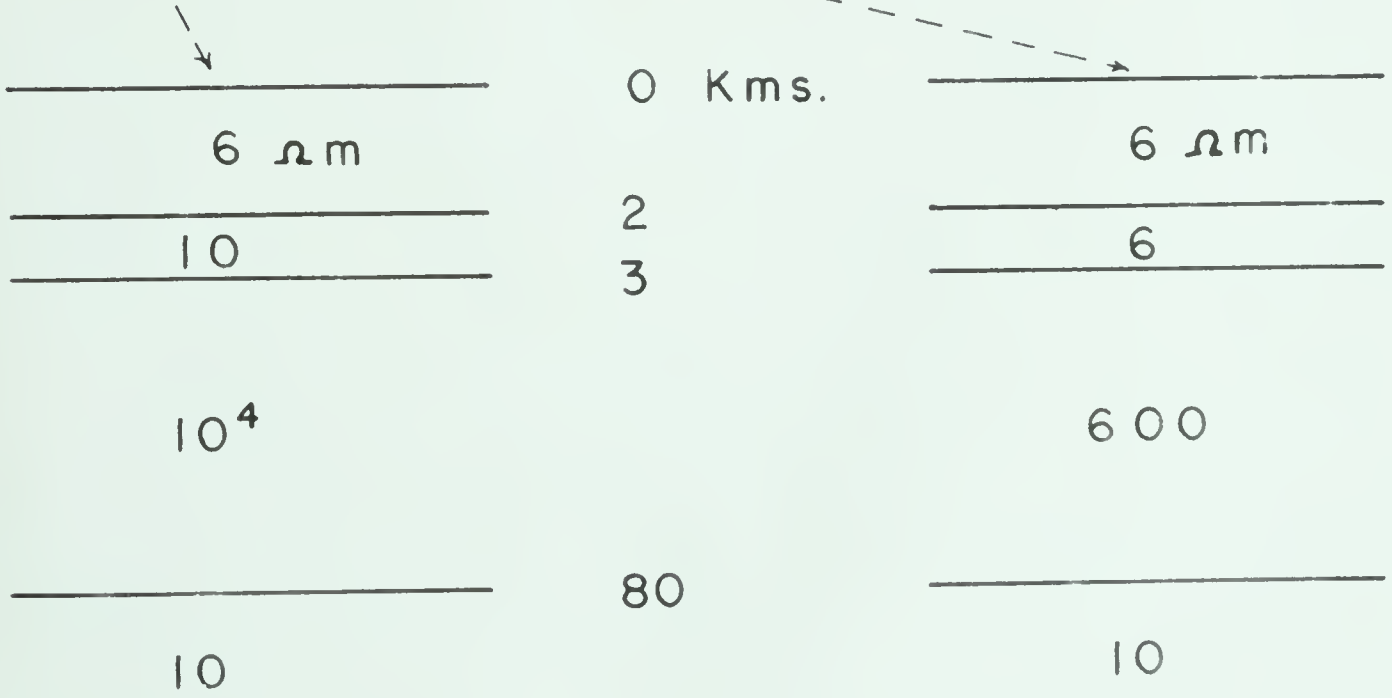

Fig. 23. Experimental and theoretical apparent resistivity curves together with models for the theoretical curves.

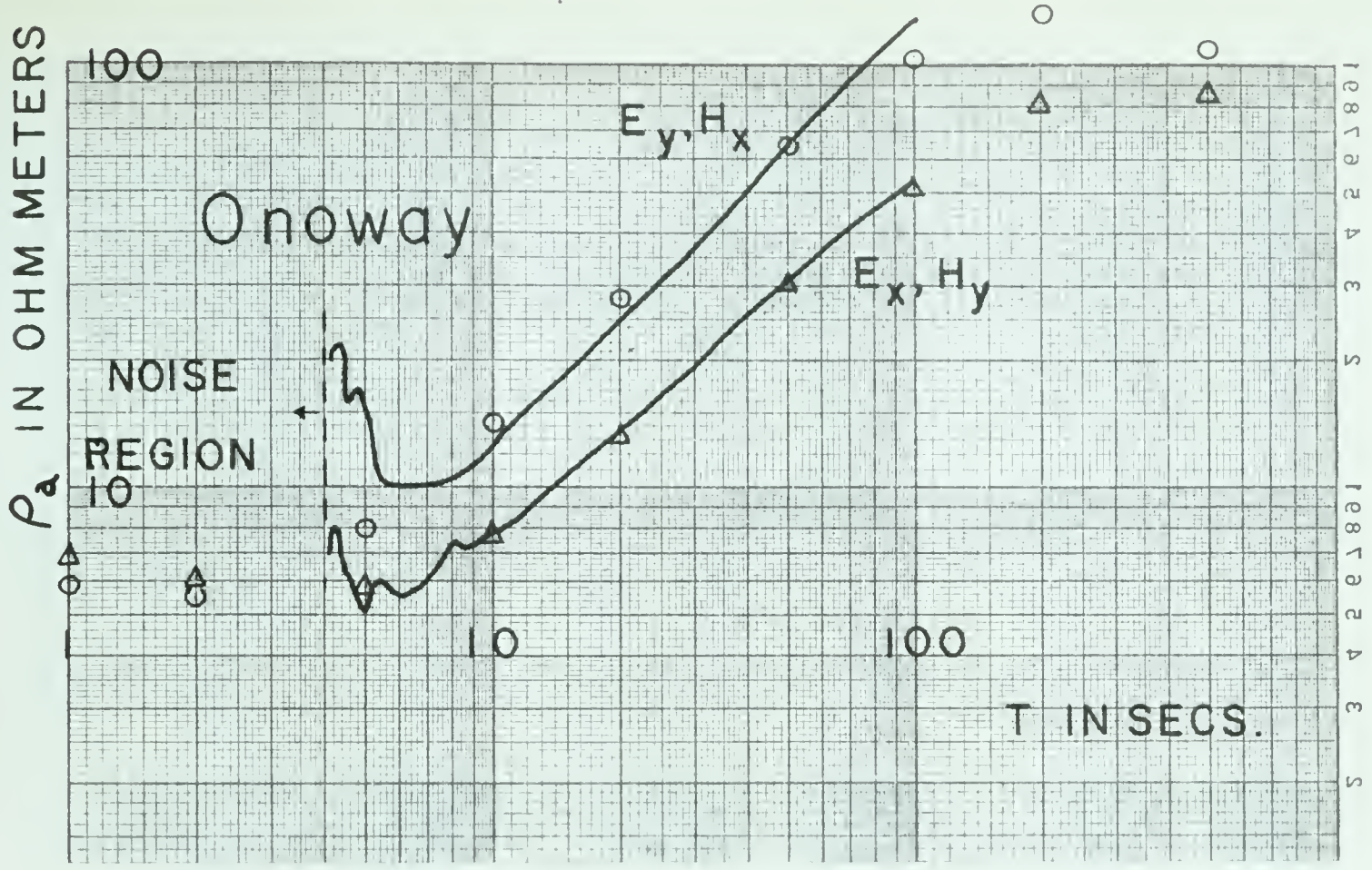

LEGEND

Solid line — Experimental Apparent Resistivity Curves

Δ and ○ — Theoretical Curves and corresponding Models

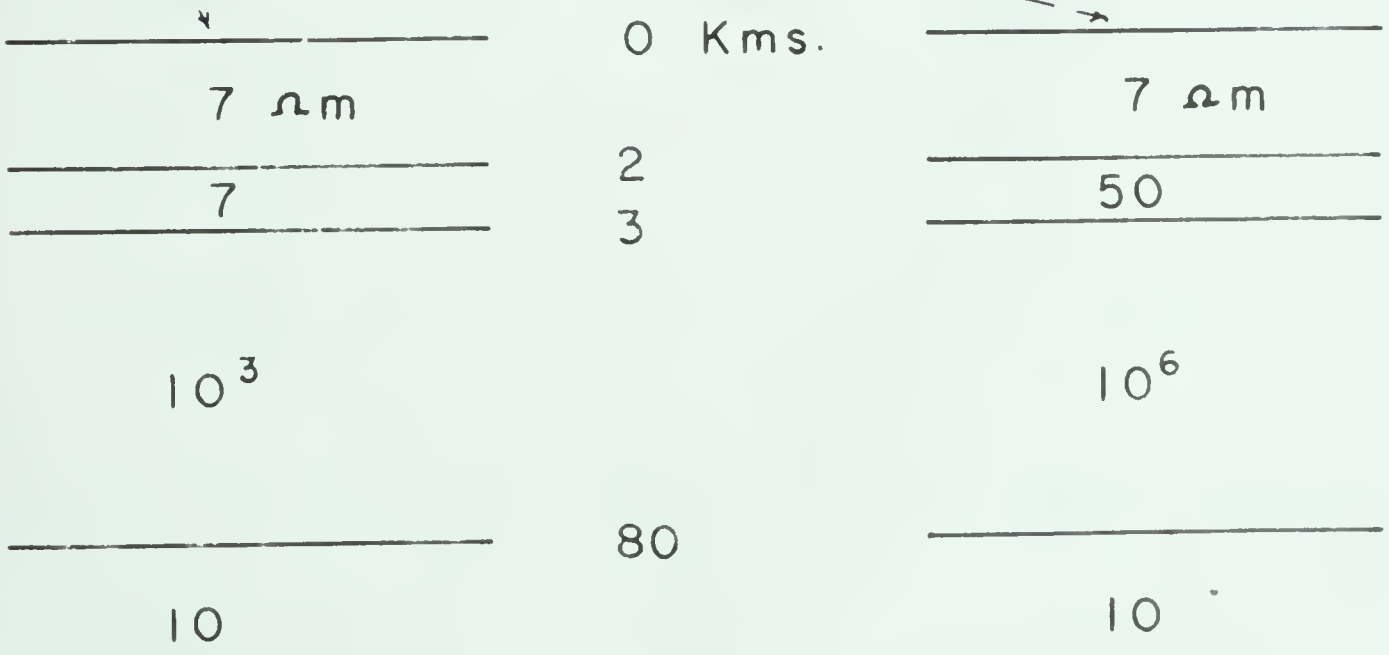

Fig. 24. Experimental and theoretical apparent resistivity curves together with models for the theoretical curves.

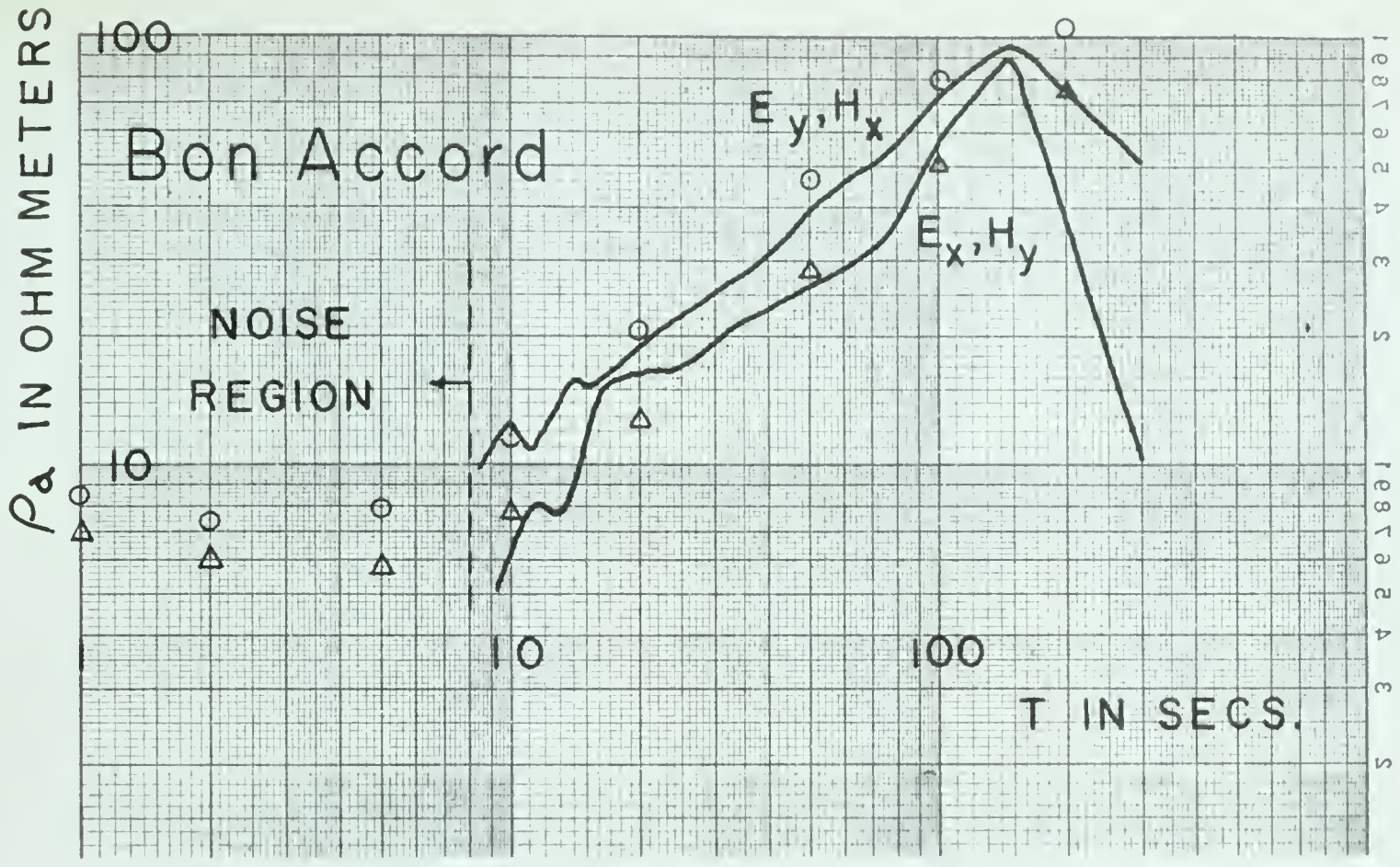

LEGEND

Solid line — Experimental Apparent Resistivity Curves

Δ and ○ — Theoretical Curves and corresponding Models

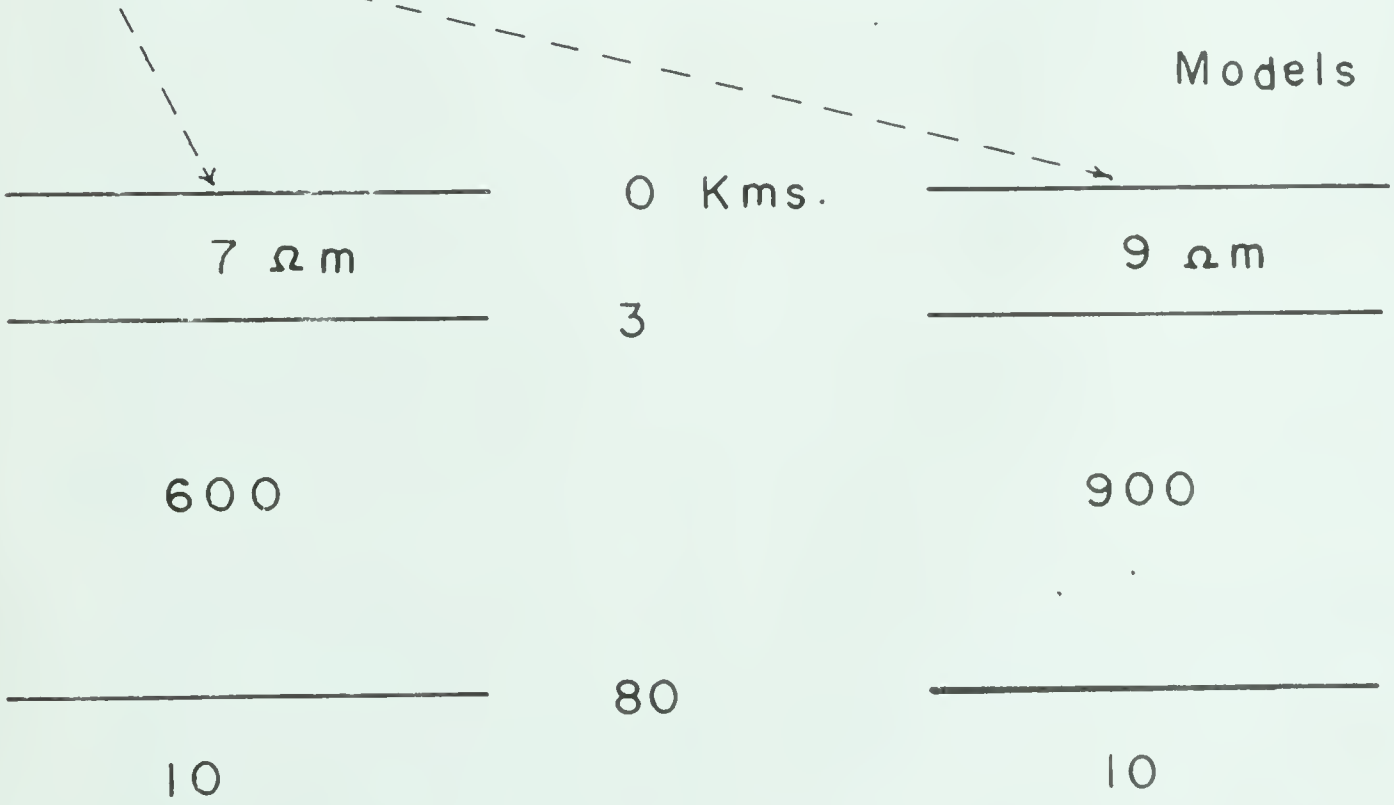

Fig. 25. Experimental and theoretical apparent resistivity curves together with models for the theoretical curves.

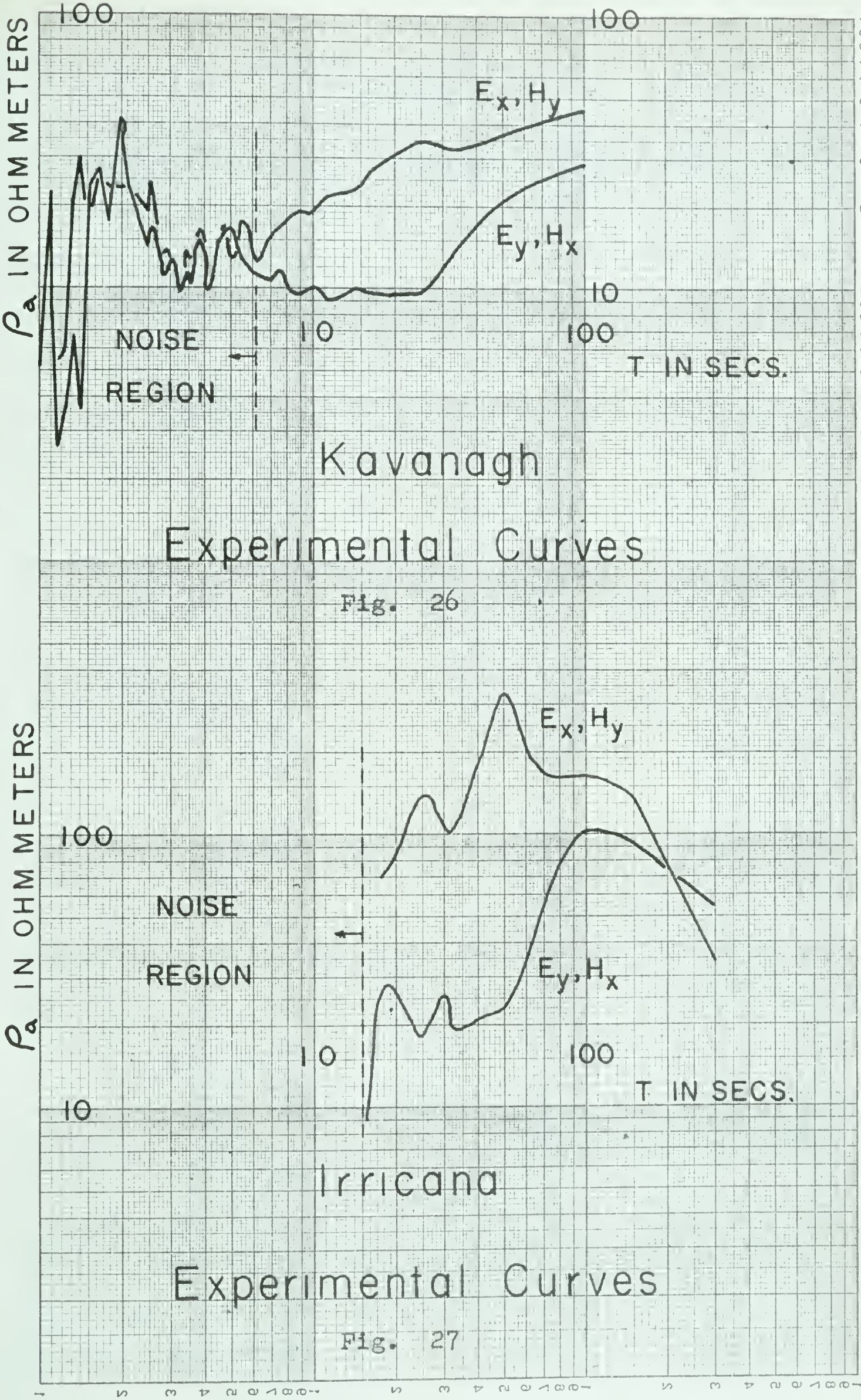

Kavanagh

Experimental Curves

Fig. 26

Irricana

Experimental Curves

Fig. 27

CONCLUSION

Theoretical apparent resistivity curves were computed for the five-layer case. This was done in order to determine the influence the sedimentary basin, which consists of rocks from five geological time divisions, has on the shape of the apparent resistivity curves.

A convenient program has been devised for obtaining experimental apparent resistivity curves. The data is recorded on magnetic tape. Then by means of a playback system, this data in analog form, is converted into digital form. This digitized data, in conjunction with programs designed to obtain power spectra and apparent resistivity curves, were fed into the electronic computor (IBM 1620 at the University of Alberta). Thus the entire data processing was done by electronic means; hence the most time-consuming part of the entire operation has been eliminated.

Interpretation of the experimental apparent resistivity curves yield values for the resistivity of the sedimentary basin which are in agreement with those from electrical logs. Resistivities ranging from 6 to 9 ohm meters were obtained for the near-surface sedimentary layers and values from 6 to 50 ohm meters for those layers near the Precambrian.

The results of this investigation indicate the crystalline basement to be anisotropic. However, more recordings, which will either confirm or repudiate this finding, are desired.

The analysis indicates that there is no electrical discontinuity at the Mohorovicic discontinuity. However, the results are suggestive of an electrical discontinuity at a depth of 80 km, which is roughly twice the depth to the Moho.

At the long periods which are required for a substratum investigation, source effects may be significant. Research into this aspect is presently being carried out at the University of Alberta. In particular, research is being conducted to determine the intrinsic impedance of the earth for dipolar fields resulting from dipoles (located above the earth's surface) of various types and orientations.

APPENDIX

Section I

PRACTICAL UNITS	CONVERSION
H measured in gammas (γ)	1 em unit = $10^5 \gamma$
E measured in $^{mv}/_{km}$.	1 em unit = 1 $^{mv}/_{km}$
Length measured in km	1 em unit = 10^{-5} km
ρ measured in ohm meters	1 em unit = 10^{-11} ohm meters

BIBLIOGRAPHY

Balser, M., and C. A. Wagner: "Observations of Earth-Ionosphere Cavity Resonances", Nature, Vol. 188, No. 4751, pp. 638-641, (1960).

Benioff, H.,: "Observations of Geomagnetic Fluctuations in the Period Range 0.3 to 120 Seconds", Jour. of Geophys. Res., Vol. 65 (May), No. 5, pp. 1413-1422, (1960).

Blackman, R. B., and J. W. Tukey,: "The Measurement of Power Spectra", Dover Publications, 190 pp., (1960).

Bossy, I., and A. DeVuyst,: "Relations Entre Les Champs Electrique et Magnetique d'une Onde de Periode tres Longue Induits dans un Milieu de Conductivite Variable", Geofisica Pura E Applicata, V44, pp. 119-134, (1959).

Burwash, R. A.,: "Reconnaissance of Subsurface Precambrian of Alberta", The Bulletin of the American Association of Petroleum Geologists, Vol. 41, No. 1, pp. 70-103, (1957).

Cagniard, L.,: "Basic Theory of the Magneto-Telluric Method of Geophysical Prospecting", Geophysics, Vol. 18, pp. 605-635, (1953).

Cantwell, T.,: "Detection and Analysis of Low Frequency Magneto-Telluric Signals", Ph. D. Thesis, Department of Geology and Geophysics, MIT, 170 pp., (1960).

Garland, G. D.,: "Earth Currents", Methods and Techniques in Geophysics, Interscience Publishers, Inc., New York, pp. 277-307, (1960).

Garland, G. D., and R. A. Burwash,: "Geophysical and Petrological Study of Precambrian of Central Alberta Canada", The Bulletin of the American Association of Petroleum Geologists, Vol. 43, No. 4, pp. 790-806, (1959).

Lahiri, B. N., and A. T. Price,: "Electromagnetic induction in non-uniform conductors, and the determination of the conductivity of the earth from terrestrial magnetic variations", Phil. Trans. Roy. Soc. London A, 237, pp. 509-540, (1939).

Neves, A. S.,: "The Magneto-Telluric Method in Two-Dimensional Structures", Ph. D. Thesis, Dept. of Geology and Geophysics, MIT, 106 pp., (1957).

Niblett, E. R., and C. Sayn-Wittgenstein,: "Variation of Electrical Conductivity with Depth by the Magneto-Telluric Method", Geophysics, Vol. XXV, No. 5, pp. 998-1008, (1960).

Price, A. T.,: "The Theory of Magnetotelluric Methods When the Source Field is Considered", Jour. Geophys. Res., Vol. 67, No. 5, pp. 1907-1918, (1962).

Richards, T. D., and D. J. Walker,: "Measurement of the Thickness of the Earth's Crust in The Albertan Plains of Western Canada", Geophysics, Vol. 24, No. 2, pp. 262-284, (1959).

Schelkunoff, S. A.,: Electromagnetic Waves, Chap. 12, D. Van Nostrand Co., New York, (1943).

Schlumberger Document - No. 8,: "Introduction to Well Logging", Schlumberger Well Surveying Corporation, 176 pp., (1958).

Schlumberger, M., and G. Kunetz,: "Variations Rapides Simultanees du Champ Tellurique en France et a Madagascar", CR. Acad. Science, Paris, 223, pp. 551-553, (1946).

Swinnerton-Dyer, H. P. F.,: "The Calculation of Power Spectra", The Computer Journal, 5, No. 1, pp. 16-23, (1962).

Wait, J. R.,: "On the Relation Between Telluric Currents and the Earth's Magnetic Field", Geophysics, Vol. XIX, No. 2, pp. 281-289, (1954).

Webster, T. F.,: "An Experimental Investigation of Telluric and Magneto-Telluric Phenomena", M. Sc. Thesis, University of Alberta, Dept. of Physics, 92 pp., (1957).

Yungul, S. H.,: "Magneto-Telluric Sounding Three-Layer Interpretation Curves", Geophysics, Vol. XXVI, No. 4, pp. 465-473, (1961).

B29801